CANCER

# Switchable immune modulator for tumor-specific activation of anticancer immunity

Yu Zhao[1,2], Yu-Qing Xie[1], Simon Van Herck[1,3], Sina Nassiri[4], Min Gao[1], Yugang Guo[1,2], Li Tang[1,2]*



**Immune stimulatory antibodies and cytokines elicit potent antitumor immunity. However, the dose-limiting systemic toxicity greatly hinders their clinical applications. Here, we demonstrate a chemical approach, termed "switchable" immune modulator (Sw-IM), to limit the systemic exposure and therefore ameliorate their toxicities. Sw-IM is a biomacromolecular therapeutic reversibly masked by biocompatible polymers through chemical linkers that are responsive to tumor-specific stimuli, such as high reducing potential and acidic pH. Sw-IMs stay inert (switch off) in the circulation and healthy tissues but get reactivated (switch on) selectively in tumor via responsive removal of the polymer masks, thus focusing the immune boosting activities in the tumor microenvironment. Sw-IMs applied to anti–4-1BB agonistic antibody and IL-15 cytokine led to equivalent antitumor efficacy to the parental IMs with markedly reduced toxicities. Sw-IM provides a highly modular and generic approach to improve the therapeutic window and clinical applicability of potent IMs in mono- and combinational immunotherapies.**

## INTRODUCTION

Immune stimulatory agonistic antibodies (e.g., anti–4-1BB) and cytokines [e.g., interleukin-15 (IL-15)] elicit potent anticancer immunity. However, their therapeutic potential is greatly hampered by the severe systemic toxicity deriving from excessive activation of immune and inflammatory responses in the circulation compartment and/or healthy tissues where the target receptors are widely present (*1*–*4*). In addition, combination therapies increase the patients' response rate to immunotherapy at the cost of exacerbated toxicities. For instance, adoptive T cell transfer (ACT) adjuvanted by supporting cytokines enhances the efficacy against solid tumors (*5*, *6*) but leads to severe, sometimes life-threatening, side effects (*7*, *8*).

To enlarge the therapeutic window of biomacromolecular immune modulators (IMs) for mono- or combinational immunotherapies, there are two general means that could be applied. One is to physically confine the IM distribution in tumor through local (*9*–*11*) or targeted (*12*–*14*) delivery. The other is to achieve selective activation of IMs in the tumor microenvironment (TME) regardless of their biodistribution. The latter has been recently applied in developing antibody prodrugs that are masked by recombinant fusion peptides (*8*, *15*–*20*) or protein domains (*21*–*23*) and unmasked specifically in the TME in response to tumor-associated proteases. These genetic engineering approaches have so far been exclusively limited on the design of protease responsiveness and applicable in a handful of antibodies or antibody fragments.

Here, we demonstrate a generalizable chemical approach, termed switchable IM (Sw-IM), which could be widely applied to a broad range of IMs including antibodies and cytokines with diverse responsiveness. IMs were reversibly blocked by biocompatible polymers through responsive covalent linkers that degraded in response to stimuli specific in the TME, such as the high reducing potential and acidic pH, to release the polymer blockades (Fig. 1). The prepared Sw-IMs remained at off status in peripheral blood and healthy tissues but rapidly switched on in the TME with regained immune stimulating activities (Fig. 1, A and B). Treatments with redox-responsive switchable anti–4-1BB antibody as a monotherapy, or a combination therapy of redox-responsive switchable IL-15 superagonist (IL-15SA) and ACT led to equivalent antitumor efficacy to the parental IMs with markedly enhanced safety profiles in mouse models of cancer. This facile and generally applicable approach allowed modular design using diverse protein therapeutics, masking polymers, and chemical linkers of different responsiveness (Fig. 1C). Analyses of a small library of Sw-IMs for their in vitro and in vivo performance enabled us to determine the favorable formulation parameters of Sw-IMs for the optimized antitumor efficacy and safety profile.

## RESULTS

### Design and preparation of Sw-IMs

To prove the concept, we first conjugated anti-trinitrophenol (TNP) antibody as a model drug with polyethylene glycol (PEG), a hydrophilic and biocompatible polymer with low immunogenicity (*24*), through a traceless redox-responsive linker bearing two amine-reactive *N*-hydroxysuccinimide (NHS) groups (fig. S1). These redox-responsive antibody-polymer conjugates, termed switchable anti-TNP, ($Sw_{redox}$aTNP; Table 1, entry 1, and table S1, entries 1 to 7) were successfully prepared evidenced by the increased molecular weight (MW) characterized by SDS–polyacrylamide gel electrophoresis (PAGE) (fig. S2A) and ultrahigh-performance liquid chromatography (UHPLC) equipped with a size exclusion chromatography (SEC) column (fig. S2B), as well as the increased sizes measured by dynamic light scattering (DLS) (fig. S2C).

Next, we focused on anti–4-1BB, an agonistic antibody that stimulates tumor necrosis factor receptor superfamily member 9 (TNFRSF-9) and is a potent cancer immunotherapy, but its clinical applications have been greatly hindered by the hepatoxicity (*25*, *26*). We prepared a series of redox-responsive switchable anti–4-1BB antibodies ($Sw_{redox}$a4-1BBs; Table 1, entries 3 to 8, and table S1, entries 8 to 13). To fine-tune the masking effects, we controlled the

[1]Institute of Bioengineering, École Polytechnique Fédérale de Lausanne (EPFL), 1015 Lausanne, Switzerland. [2]Institute of Materials Science & Engineering, EPFL, 1015 Lausanne, Switzerland. [3]Department of Pharmaceutics, Ghent University, 9000 Ghent, Belgium. [4]Bioinformatics Core Facility, SIB Swiss Institute of Bioinformatics, 1015 Lausanne, Switzerland.
*Corresponding author. Email: li.tang@epfl.ch

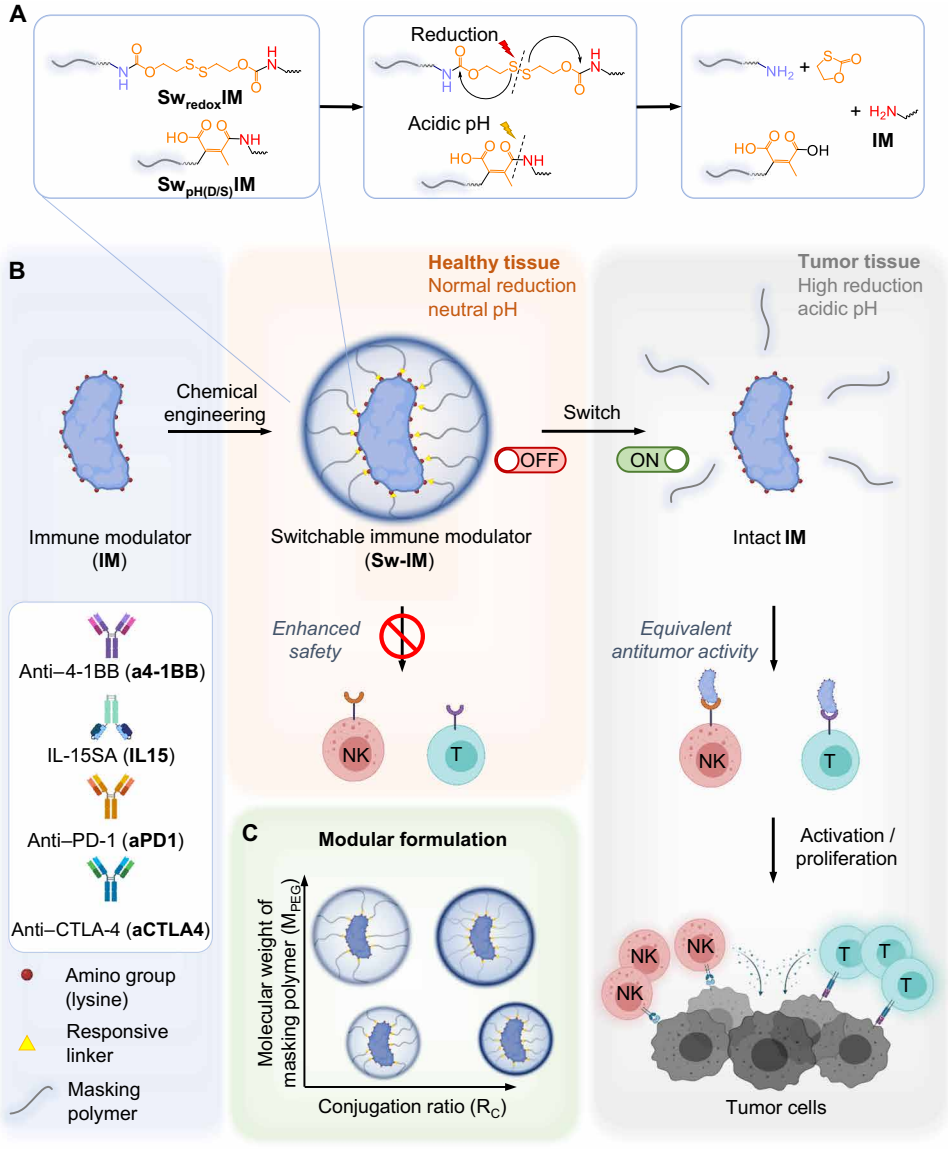


**Fig. 1. Design of Sw-IMs.** (**A**) Chemical structures and responsive switch on of redox- and acidic pH–responsive Sw-IMs. $Sw_{redox}$IM, redox-responsive Sw-IM; $Sw_{pH(D/S)}$IM, acidic pH–responsive Sw-IM with dibenzocyclooctyne (DBCO) or thioether spacer. (**B**) Schematic illustration of the preparation and in vivo fate of Sw-IMs. Sw-IMs remain switched off in the circulation and healthy tissues and get switched on specifically in the TME to stimulate proliferation and effector functions of $CD8^+$ T cells and NK cells for cancer immunotherapy. (**C**) Modular design of Sw-IMs by tuning the conjugation ratio ($R_C$) and MW ($M_{PEG}$) of masking polymers. $R_C$ is defined as the percentage of conjugated amino groups among all the detectable amino groups of an IM.

degree of modification density and the MW of PEG ($M_{PEG}$) for conjugation. By varying the feeding mole ratios of PEG to antibody ($R_F$), the percentage of conjugated amino groups among all the detectable amino groups of the antibody molecule (termed conjugation ratio, $R_C$) can be tuned (Fig. 2A and Table 1, entries 3 to 8), which was determined by the 2,4,6-trinitrobenzenesulfonic acid (TNBSA) assay (fig. S3) (*27*). A higher $R_F$ generally resulted in a higher $R_C$; the maximal $R_C$ is limited by certain number of reactive amino groups per antibody molecule (maximal $R_C$ = 83.1% for $Sw_{redox}$a4-1BBs; table S1, entry 11). For example, anti–4-1BB antibody conjugated with PEG ($M_{PEG}$ = 10 kDa) with an $R_F$ of 50 ($Sw_{redox}$a4-$1BB_{10k\text{-}50}$) resulted in an $R_C$ of 61.8%, while the $R_C$ value of $Sw_{redox}$a4-$1BB_{10k\text{-}100}$ was 73.9%. In addition, a higher $M_{PEG}$ led to a lower $R_C$ because of reduced reactivity and increased steric hindrance during reaction (Fig. 2A and Table 1, entries 3, 5, and 7 and entries 4, 6, and 8). $Sw_{redox}$a4-1BBs showed larger MWs compared to the native anti–4-1BB antibody characterized by both SDS-PAGE and UHPLC (Fig. 2, B and C). Similarly, the hydrodynamic dimeter of $Sw_{redox}$a4-1BBs increased as measured by DLS (fig. S4A).

The syntheses of the chemically modified switchable antibodies can be readily extended to other immunoglobulin G (IgG) antibodies in addition to anti-TNP and anti–4-1BB antibodies, such as checkpoint blockade antibodies against programmed cell death protein 1 (anti–PD-1) ($Sw_{redox}$aPD-1 s; Table 1, entry 9, fig. S5A, and table S1, entries 14 to 21) and cytotoxic T lymphocyte–associated protein 4 (anti–CTLA-4) ($Sw_{redox}$aCTLA4s; Table 1, entry 10, fig. S5B, and

**Table 1. Preparation and characterizations of Sw-IMs.** Sw-IM, switchable immune modulator (Sw-IM is denoted as $Sw_{linker}protein_{MPEG\text{-}RF}$); redox, redox-responsive linker; pH(D), acidic pH–responsive linker with a DBCO-triazole spacer; pH(S), acidic pH–responsive linker with a thioether spacer; aTNP, anti-TNP antibody; a4-1BB, anti–4-1BB antibody; aPD-1, anti–PD-1 antibody; aCTLA4, anti–CTLA-4 antibody; IL15, IL-15SA; SS, disulfate linker; S, thioether; $M_{PEG}$, MW of PEG; $R_F$, feeding mole ratio of PEG to IM; $R_C$, conjugation ratio, defined as (number of conjugated $NH_2$ groups/total number of $NH_2$ groups of IM) × 100%.

| Entry | Sw-IM | IM | Linker* | $M_{PEG}$ (Da) | $R_F$ | $R_C$ (%) | Size (nm)† | $EC_{50}$ off (nM)‡ | $EC_{50}$ on (nM)‡ |
|---|---|---|---|---|---|---|---|---|---|
| 1 | $Sw_{redox}aTNP_{10k\text{-}100}$ | Anti-TNP | SS | 10k | 100 | 59.5 | 8.2 ± 2.2 | | |
| 2 | a4-1BB | Anti–4-1BB | | | | | 5.5 ± 1.4 | | 0.077 |
| 3 | $Sw_{redox}a4\text{-}1BB_{5k\text{-}50}$ | Anti–4-1BB | SS | 5k | 50 | 66.8 | 7.3 ± 2.1 | | |
| 4 | $Sw_{redox}a4\text{-}1BB_{5k\text{-}100}$ | Anti–4-1BB | SS | 5k | 100 | 78.9 | 8.7 ± 2.4 | 5.6 | 0.41 |
| 5 | $Sw_{redox}a4\text{-}1BB_{10k\text{-}50}$ | Anti–4-1BB | SS | 10k | 50 | 61.8 | 8.0 ± 2.3 | 1.2 | 0.30 |
| 6 | $Sw_{redox}a4\text{-}1BB_{10k\text{-}100}$ | Anti–4-1BB | SS | 10k | 100 | 73.9 | 8.5 ± 2.3 | 2.9 | 0.77 |
| 7 | $Sw_{redox}a4\text{-}1BB_{20k\text{-}50}$ | Anti–4-1BB | SS | 20k | 50 | 54.6 | 7.6 ± 2.2 | 1.3 | 0.29 |
| 8 | $Sw_{redox}a4\text{-}1BB_{20k\text{-}100}$ | Anti–4-1BB | SS | 20k | 100 | 70.6 | 10.4 ± 3.0 | | |
| 9 | $Sw_{redox}aPD1_{10k\text{-}100}$ | Anti–PD-1 | SS | 10k | 100 | 62.3 | 8.3 ± 2.3 | 3.8 | 1.7 |
| 10 | $Sw_{redox}aCTLA4_{10k\text{-}100}$ | Anti–CTLA-4 | SS | 10k | 100 | 55.6 | 8.5 ± 2.1 | | |
| 11 | IL15 | IL-15SA | | | | | 9.8 ± 2.2 | | 7.8 |
| 12 | $Sw_{redox}IL15_{5k\text{-}100}$ | IL-15SA | SS | 5k | 100 | 64.2 | 13.8 ± 3.1 | 54.2 | 10.5 |
| 13 | $Sw_{redox}IL15_{10k\text{-}50}$ | IL-15SA | SS | 10k | 50 | 35.7 | 13.3 ± 3.5 | 22.0 | 10.4 |
| 14 | $Sw_{redox}IL15_{10k\text{-}100}$ | IL-15SA | SS | 10k | 100 | 56.5 | 14.9 ± 4.1 | 38.7 | 11.7 |
| 15 | $Sw_{redox}IL15_{20k\text{-}50}$ | IL-15SA | SS | 20k | 50 | 35.5 | 12.5 ± 3.1 | 27.4 | 10.5 |
| 16 | $Sw_{pH(D)}a4\text{-}1BB_{5k\text{-}400}$ | Anti–4-1BB | DBCO | 5k | 400 | 81.2 | 10.3 ± 3.2 | 1.4 | 0.40 |
| 17 | $Sw_{pH(S)}a4\text{-}1BB_{5k\text{-}400}$ | Anti–4-1BB | S | 5k | 400 | 54.3 | 8.0 ± 2.4 | 1.2 | 0.082 |

*The chemical structure of the linkers is shown in fig. S1. †Hydrodynamic diameter measured by dynamic light scattering. ‡Half-maximal effective concentration values ($EC_{50}$s) of Sw-IMs at off and on status determined by $CD8^+$ T cell binding assay.

table S1, entries 22 to 29), showing excellent modularity of this method. In addition to antibody therapeutics, we next extended the method further to the fabrication of switchable cytokines. We used IL-15SA, which is a fusion protein of IL-15, IL-15 receptor α (IL-15Rα), and a mouse IgG2c Fc, for the conjugation with PEG in a similar way to switchable antibodies ($Sw_{redox}$IL15s; Table 1, entries 12 to 15, and table S1, entries 30 to 41). The $R_C$ values, MWs, and sizes can be controlled similarly to afford $Sw_{redox}$IL15s of various MW and sizes (Fig. 2, D to F, and fig. S4B).

The responsiveness of Sw-IMs can also be modularly controlled using linkers responsive to diverse stimuli. Acidic pH is another chemical characteristic in the TME (*28*). We next designed and prepared acidic pH–responsive Sw-IMs using linkers bearing methylmaleic anhydride (MMA), an acid-labile amine-reacting moiety (Fig. 1A) (*29*). The amino groups of an IM could be first modified with a small-molecule linker, azidomethyl methylmaleic anhydride (AzMMMA), and further conjugated with dibenzocyclooctyne (DBCO)–functionalized PEG (mPEG-DBCO) via copper-free click reaction ($Sw_{pH(D)}$a4-1BB; Table 1, entry 16, fig. S6, and table S1, entries 42 and 43). Alternatively, we could first prepare the MMA-functionalized PEG (mPEG-MMMA) followed by conjugating mPEG-MMMA to IMs ($Sw_{pH(S)}$a4-1BB; Table 1, entry 17, and fig. S7). Much higher $R_F$ was necessary to reach similar $R_C$ because of the lower reaction activity of maleic anhydrides with amino groups comparing to NHS esters in the preparation of redox-responsive Sw-IMs. pH-responsive Sw-IMs of various $R_C$ and $M_{PEG}$ were prepared and characterized similarly (fig. S8).

## Controlled switch off and on of Sw-IMs

To validate the responsiveness, $Sw_{redox}$a4-1BBs and $Sw_{redox}$IL15s were treated with L-glutathione (GSH) mimicking the reducing environment in the TME (*30*). Compared to the nonreduced Sw-IMs (off status), the reduced Sw-IMs (on status) exhibited largely decreased $R_C$ values, revealing liberation of free amino groups and thus successful responsive removal of the masking polymers (Fig. 2, A and D). The reduced Sw-IMs also had lowered MWs, which were close to that of the native IMs as characterized by the SDS-PAGE gels (Fig. 2, B and E). However, there were residual PEG polymers that were not completely removed in the set reducing condition. More potent reducing condition could not only potentially remove fully the residue-conjugated polymers but also lead to cleavage of disulfide bonds in the hinge region and degradation of the proteins. Similarly to the redox responsive Sw-IMs, the PEG masks of pH-responsive $Sw_{pH(D)}$a4-1BBs and $Sw_{pH(S)}$a4-1BBs could be removed in response to the acidic pH (fig. S8, A and B).

Next, to assess the biological functions of Sw-IMs upon responsive reactivation, we first determined their binding capacity toward activated $CD8^+$ T cells, which expressed a variety of surface receptors including 4-1BB and IL-15R (Fig. 2G) (*31*–*33*). The binding capability of fluorescently labeled Sw-IMs toward activated $CD8^+$ T cell was determined by measuring the mean fluorescence intensities (MFIs) with flow cytometry. Sw-IMs at off status exhibited markedly reduced affinity compared to the native IMs, while the reactivated Sw-IMs (on status) showed completely or partially recovered binding capacity (Fig. 2, H to K). $Sw_{redox}$a4-1BBs at off status exhibited

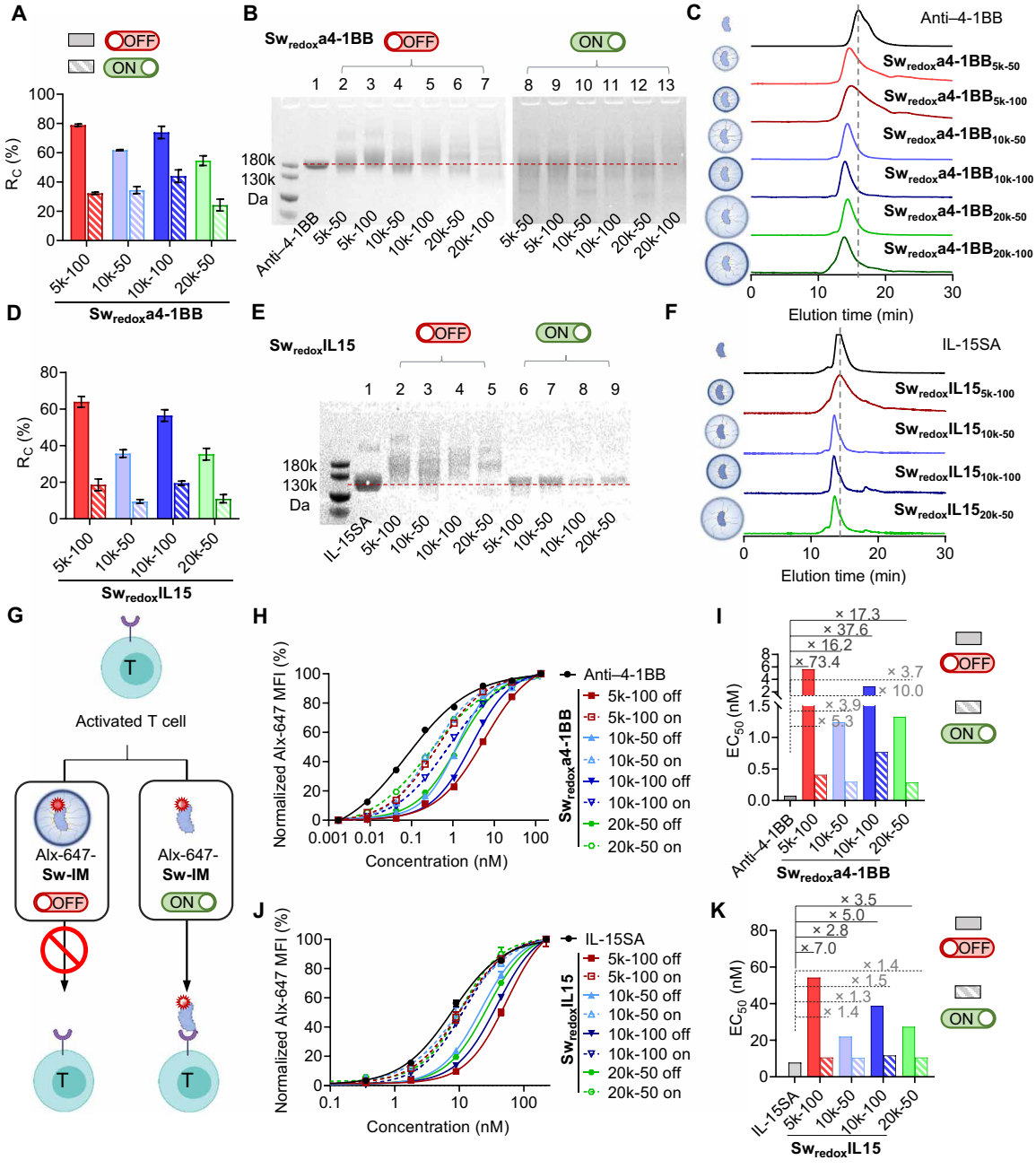


**Fig. 2. Stimuli-responsive switch on of Sw-IMs.** (**A**) $R_C$ values of $Sw_{redox}$a4-1BBs at off and on status. (**B**) $Sw_{redox}$a4-1BBs at off and on status were analyzed by SDS-PAGE. (**C**) Traces of $Sw_{redox}$a4-1BBs measured by UHPLC equipped with a SEC column. (**D**) $R_C$ values of $Sw_{redox}$IL15s at off and on status. (**E**) $Sw_{redox}$IL15s at off and on status were analyzed by SDS-PAGE. (**F**) UHPLC-SEC traces of $Sw_{redox}$IL15s. The dashed lines indicate the molecular (B and E) or elution time (C and F) of native IMs. (**G**) Schematic illustration of $CD8^+$ T cell binding assay. Activated $CD8^+$ T cells ($1 \times 10^5$) were incubated with Alexa Fluor-647 (Alx-647)–labeled Sw-IMs at off or on status at series diluted concentrations for 1 hour. Mean fluorescence intensity (MFI) of $CD8^+$ T cells was measured by flow cytometry to represent the binding capacity. (**H**) Binding capacity of $Sw_{redox}$a4-1BBs at off and on status with $CD8^+$ T cells. The plot is a representative of three independent experiments. (**I**) Half-maximal effective concentrations ($EC_{50}$s) of $Sw_{redox}$a4-1BBs at off and on status. (**J**) Binding capacity of $Sw_{redox}$IL15s at off and on status with $CD8^+$ T cells. The plot is a representative of three independent experiments. (**K**) $EC_{50}$s of $Sw_{redox}$IL15s at off and on status.

the half-maximal effective concentration ($EC_{50}$) values 16.2- to 73.4-fold higher than the native anti–4-1BB antibody, indicating low/none biological activities; recovered $Sw_{redox}$a4-1BBs (on status) had comparable $EC_{50}$ values to that of the native anti–4-1BB antibody (Fig. 2I). The partial recovery of the binding activities of $Sw_{redox}$a4-1BBs was possibly due to the incomplete removal of the masking polymers in the set reducing condition and the degradation of part of the antibodies (*34*). $EC_{50}$ values of $Sw_{redox}$IL15s showed the similar trend, suggesting the inactivity of masked IL-15SA and the almost fully regained affinity at on status (with

$EC_{50}$ values 1.3- to 1.5-fold higher than those of the native) (Fig. 2, J and K).

In general, at off status, Sw-IMs with higher $R_C$ (e.g., $Sw_{redox}a4\text{-}1BB_{10k\text{-}50}$, $EC_{50}$ off = 1.2 nM versus $Sw_{redox}a4\text{-}1BB_{10k\text{-}100}$, $EC_{50}$ off = 2.9 nM) or higher $M_{PEG}$ (e.g., $Sw_{redox}IL15_{10k\text{-}50}$, $EC_{50}$ off = 22.0 nM versus $Sw_{redox}IL15_{20k\text{-}50}$, $EC_{50}$ off = 27.4 nM) showed higher $EC_{50}$ values, implying that increased masking effects resulted in less activities of Sw-IMs (Table 1, entries 5, 6, 13, and 15). Exceptions were $Sw_{redox}a4\text{-}1BB_{5k\text{-}100}$ and $Sw_{redox}IL15_{5k\text{-}100}$, which had very high $EC_{50}$ values at off status (73.4- and 7.0-fold higher than those of the native IMs, respectively), although they were conjugated with the shortest PEG polymer chain ($M_{PEG}$ = 5 kDa) (Fig. 2, I and K). In addition, redox-responsive switchable anti–PD-1 antibodies ($Sw_{redox}aPD1$) and acid pH–responsive switchable anti–4-1BB antibodies ($Sw_{pH(D)}a4\text{-}1BBs$ and $Sw_{pH(S)}a4\text{-}1BBs$) can be controlled similarly at off and on status in response to the corresponding stimuli (Table 1, entries 9, 16, and 17, and fig. S9). We also examined the functional activities of Sw-IMs at off and on status in activating $CD8^+$ T cell in vitro in addition to the binding assay (fig. S10). $Sw_{redox}a4\text{-}1BB$ and $Sw_{redox}IL15$ exhibited much higher $EC_{50}$ values at off status but recovered the functional activities at on status. Together, the structural and functional assays provide evidence that Sw-IMs could regain the biological activities upon triggered removal of the masking polymers.

## Selective switch on of Sw-IMs in the TME leading to antitumor immunity

Next, we examined whether the Sw-IMs were switched on in the TME by evaluating their immune stimulation and antitumor activities in vivo. C57BL/6 mice bearing subcutaneous MC38 murine colon adenocarcinoma, a model known to be responsive to costimulatory antibody therapy (*35*), received intraperitoneal injections of $Sw_{redox}a4\text{-}1BBs$ of different formulations as compared to the native anti–4-1BB antibody (Fig. 3A). $Sw_{redox}a4\text{-}1BBs$ showed equivalent tumor growth control compared to the native anti–4-1BB antibody except $Sw_{redox}a4\text{-}1BB_{5k\text{-}100}$ (Fig. 3, B and C, and fig. S11A). We further analyzed the immune cell infiltrates in tumor and their phenotypes to determine the activities of Sw-IMs for immune activation in the TME. Correlating with the induced tumor regression, all the $Sw_{redox}4\text{-}1BBs$ but $Sw_{redox}a4\text{-}1BB_{5k\text{-}100}$ enhanced the tumor infiltration of $CD8^+$ T cells to a comparable degree to the native anti–4-1BB antibody (Fig. 3, D and E). Furthermore, $Sw_{redox}a4\text{-}1BB_{10k\text{-}50}$, $Sw_{redox}a4\text{-}1BB_{10k\text{-}100}$, and $Sw_{redox}a4\text{-}1BB_{20k\text{-}50}$ elicited similarly enhanced effector functions of intratumoral $CD8^+$ lymphocytes to the native anti–4-1BB antibody evidenced by the frequency of interferon-γ (IFN-γ)–secreting $CD8^+$ T cells (59.3, 78.1, and 73.8%, respectively, as compared to 75.3% of the native anti–4-1BB antibody) (Fig. 3F). $Sw_{redox}a4\text{-}1BB_{5k\text{-}100}$ showed the minimum immune activation and therapeutic efficacy likely due to the very dense PEG masking ($R_C$ = 78.9%).

We next assessed the antitumor activity of $Sw_{redox}IL15$ in combination with ACT in C57BL/6 mice bearing subcutaneous B16F10 tumors, a poorly immunogenic murine melanoma model (Fig. 3G). We focused on $Sw_{redox}IL15_{10k\text{-}100}$, as $Sw_{redox}a4\text{-}1BB$ of the same formulation ($Sw_{redox}a4\text{-}1BB_{10k\text{-}100}$) exhibited the highest antitumor activity among the $Sw_{redox}4\text{-}1BBs$ tested. ACT of Pmel T cells alone through intravenous administration showed modest effect in tumor growth control (Fig. 3H and fig. S11B). Although the combination of Pmel T cells and the native IL-15SA enhanced the tumor suppression, severe toxicities were noticed with four of five treated mice sacrificed due to more than 10% body weight loss (Fig. 3, H and I, and fig. S11C). By contrast, the combination of Pmel T cells and $Sw_{redox}IL15_{10k\text{-}100}$ prominently enhanced the tumor regression compared to ACT alone without any overt toxicities, showing a 1.4-fold increase in median survival time relative to animals receiving Pmel T cells plus the native IL-15SA (Fig. 3I). Lymphodepletion before ACT is widely applied in the clinic to enhance the engraftment of adoptively transferred cells by eliminating the competition of endogenous lymphocytes (*36*). With lymphodepletion, $Sw_{redox}IL15_{10k\text{-}100}$ combined with ACT exhibited comparable tumor growth suppression as the combination of native IL-15SA and ACT, suggesting regained immune stimulation activities in the TME (fig. S12). Noticeably, $Sw_{redox}IL15_{10k\text{-}100}$ also improved the safety in this therapeutic regimen and led to prolonged survival of tumor-bearing mice (fig. S12, C and D).

## Sw-IMs improve the safety of mono- and combinational immunotherapies

The prolonged survival of treated mice motivated us to investigate the safety profile of Sw-IMs as compared to that of the native IMs. Mice bearing tumors were treated following the dosing scheme as shown in Fig. 3A and sacrificed on day 16 for toxicity assessment. The treatment with native anti–4-1BB antibody induced evident splenomegaly, whereas the $Sw_{redox}a4\text{-}1BB$ treatment mitigated this effect (Fig. 4A). Histopathological analyses of spleen tissues showed indistinct boundaries between the red and white pulps in the spleens of mice receiving native anti–4-1BB antibody. By contrast, architecture of spleen tissues remained intact in mice receiving $Sw_{redox}a4\text{-}1BBs$ (Fig. 4B). Nonspecific expansion of splenic effector immune cells, especially $CD8^+$ T cells, leads to excessive production of IFN-γ that causes the splenomegaly accompanied by dissolution of typical histological architecture (*37*–*39*). We therefore analyzed the $CD8^+$ T cells in spleen using flow cytometry. The treatment with native anti–4-1BB antibody notably expanded the effector memory $CD8^+$ T cells ($T_{EM}$; $CD44^{high}CD62L^{low}$) (Fig. 4, C and D), $CD8^+$ T cells expressing the early activation marker CD69 (Fig. 4E), and $CD8^+$ T cells secreting granzyme B (GrzmB) or IFN-γ (Fig. 4F and fig. S13A) compared to the phosphate-buffered saline (PBS) treatment. The agonistic antibodies administered in the form of $Sw_{redox}a4\text{-}1BBs$ reduced the nonspecific expansion of effector and cytotoxic T cells in spleen that was induced by the native anti–4-1BB antibody showing enhanced safety profile.

Immunotoxicity often leads to liver damage (*40*, *41*). Upon systemic immune activation by the intraperitoneally administered native anti–4-1BB antibody, substantial mononuclear cells accumulated around the liver portal area, as shown in the images of histological analyses (Fig. 4B). By contrast, treatment with $Sw_{redox}a4\text{-}1BBs$ resulted in minimum mononuclear cell accumulation in liver. The native anti–4-1BB antibody induced substantially increased frequency and counts of $CD8^+$ T cells in liver compared to the PBS treatment, while the $Sw_{redox}a4\text{-}1BB$ treatments elicited less liver-infiltrating $CD8^+$ T cells as compared to the native antibody therapy showing alleviated toxicity (Fig. 4, G and H). Activated liver-infiltrating $CD8^+$ T cells ($CD69^+$ or $CD44^+$) were also expanded by native anti–4-1BB antibody but significantly less by $Sw_{redox}a4\text{-}1BBs$ (Fig. 4I and fig. S13B). Further, treatment in the form of $Sw_{redox}a4\text{-}1BBs$, in particular, $Sw_{redox}a4\text{-}1BB_{10k\text{-}100}$, resulted in reduced cytotoxic and cytokine-secreting $CD8^+$ T cells in liver, with 72 and 75% lower counts of liver-infiltrating $GrzmB^+$ and IFN-$\gamma^+CD8^+$ T cells compared to the native anti–4-1BB antibody, respectively (Fig. 4J and fig. S13C). The

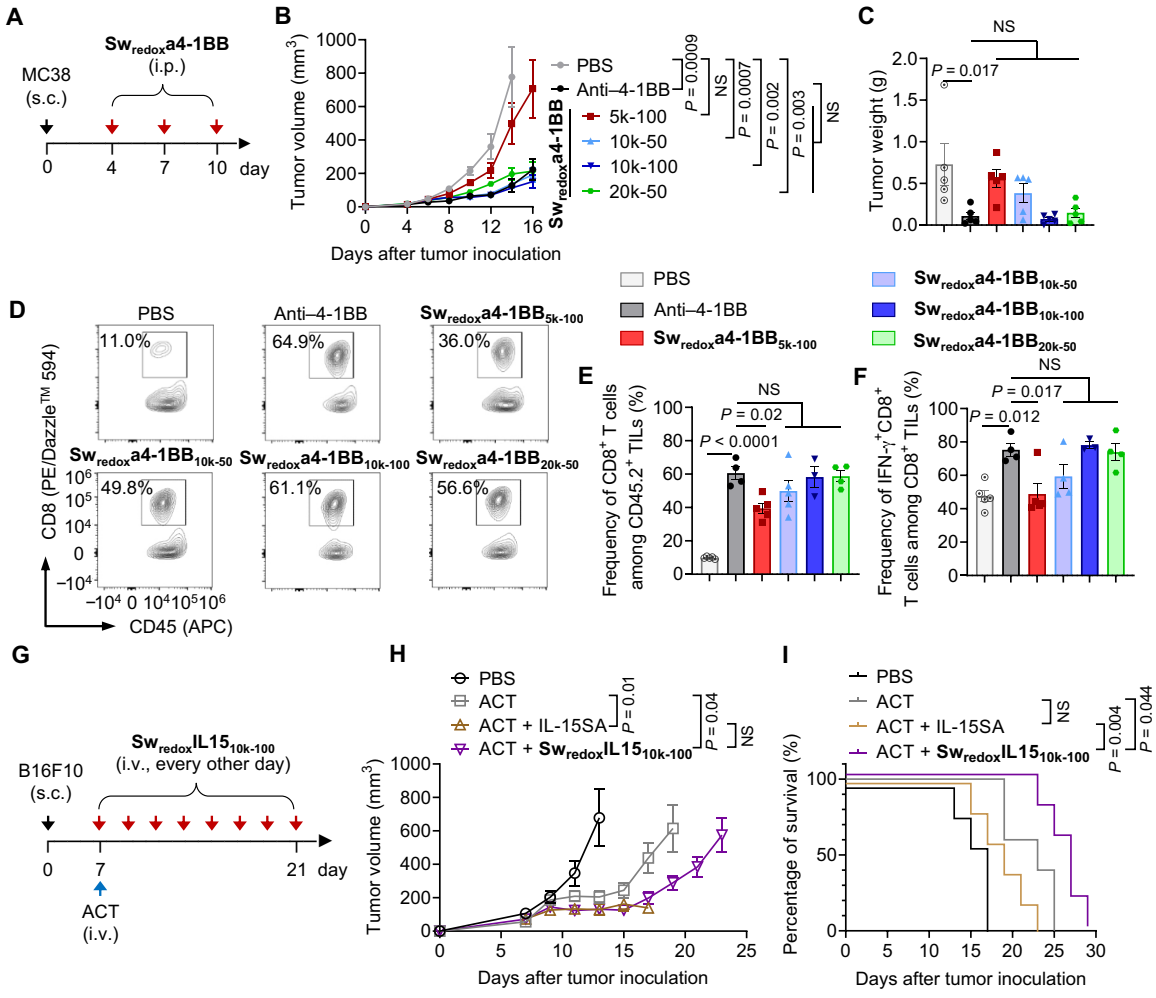


**Fig. 3. Selective switch on of Sw-IMs in the TME leading to equivalent antitumor immunity to the native IMs.** (**A** to **F**) C57BL/6 mice were inoculated subcutaneously (s.c.) with MC38 murine colon adenocarcinoma tumor cells ($2 \times 10^5$) and received intraperitoneal (i.p.) administration of native anti–4-1BB (100 μg), $Sw_{redox}$a4-1BBs (equivalent dose of anti–4-1BB), or phosphate-buffered saline (PBS) on days 4, 7, and 10. Mice were euthanized on day 16, and the tumors were processed and analyzed by flow cytometry ($n = 5$ mice). (B) Average tumor growth curves. (C) Average tumor weight on day 16. (D) Representative flow cytometry plots showing the frequencies of $CD8^+$ T cells among $CD45.2^+$ tumor-infiltrating lymphocytes (TILs). (E) Average frequencies of $CD8^+$ T cell among $CD45.2^+$ TILs. (F) Average frequencies of interferon-γ (IFN-γ)–secreting $CD8^+$ T cells among $CD8^+$ TILs. (**G** to **I**) C57BL/6 mice were inoculated subcutaneously with B16F10 murine melanoma cells ($5 \times 10^5$) and received ACT of activated Pmel $Thy1.1^+CD8^+$ T cells ($1 \times 10^7$) on day 7 followed by intravenous (i.v.) administration of native IL-15SA (5 μg), $Sw_{redox}IL15_{10k\text{-}100}$ (equivalent dose of IL-15SA), or PBS every other day from day 7 to day 21 ($n = 5$ mice). (H) Average tumor growth curves. (I) Survival curves. All data represent the mean ± SEM and are analyzed by one-way analysis of variance (ANOVA) or log-rank test; NS, not significant ($P > 0.05$).

native anti–4-1BB antibody induced elevated serum levels of liver enzyme alanine transaminase (ALT) and systemic proinflammatory cytokine (IFN-γ), a side effect also reported in the clinic with typically higher severity in patients than mice (*1*). However, this liver toxicity was not observed in mice treated with $Sw_{redox}$a4-1BBs, suggesting the alleviation of systemic immunotoxicity (Fig. 4, K and L).

We next evaluated the toxicity of $Sw_{redox}$IL15s in a combination therapy with ACT. Mice bearing subcutaneous B16F10 tumors were treated with intravenous administration of Pmel T cells alone, or Pmel T cells adjuvanted by the native IL-15SA or $Sw_{redox}IL15_{10k\text{-}100}$. Mice were sacrificed on day 14 for toxicity assessment (Fig. 5A). Treatment of ACT plus the native IL-15SA induced pronounced splenomegaly, which were greatly alleviated in mice receiving ACT plus $Sw_{redox}IL15_{10k\text{-}100}$ (Fig. 5, B and C). The observed splenomegaly was likely due to the massive expansion of both $CD8^+$ T cells and nature killer (NK) cells in spleen by the native IL-15SA (Fig. 5, D, K, and L, and fig. S14A) (*3*). Among the splenic $CD8^+$ T cells, activated $CD69^+CD8^+$ T cells, effector memory $CD8^+$ T cells ($T_{EM}$), and $CD8^+$ T cells secreting GrzmB and IFN-γ were all prominently expended by the native IL-15SA (Fig. 5, E and F, and fig. S14, B and C). On the contrary, ACT adjuvanted by $Sw_{redox}IL15_{10k\text{-}100}$ elicited no significant change of counts of splenic $CD8^+$ T cells, NK cells, or any of these $CD8^+$ T cell subsets as compared to ACT alone. In addition, treatment of ACT supported by the native IL-15SA caused liver injury evidenced by the elevated serum level of ALT (Fig. 5G). This combination therapy nonspecifically expanded the liver-infiltrating $CD8^+$ T cells, activating $CD8^+$ T cells ($CD69^+$ and $CD44^+$), $CD8^+$ T cells secreting GrzmB and IFN-γ, and NK cells (Fig. 5, H to K and M, and fig. S14, D to F). When ACT was combined with $Sw_{redox}IL15_{10k\text{-}100}$, no overt toxicity was observed in liver; the counts of total liver-infiltrating lymphocytes

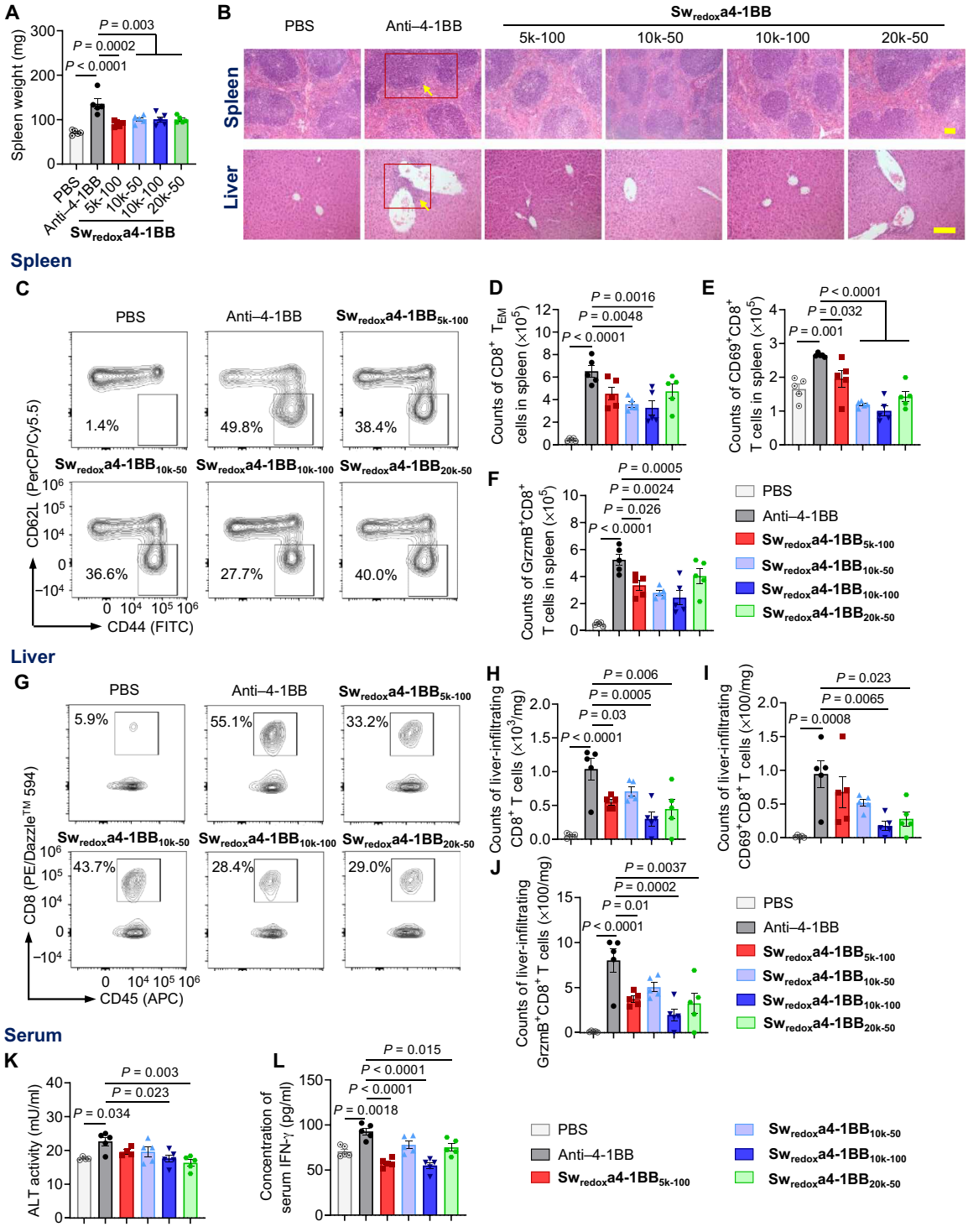


**Fig. 4. Sw-IM reduced the toxicity of anti–4-1BB agonistic antibody therapy.** C57BL/6 mice bearing MC38 tumor were treated as shown in Fig. 3A. Mice were euthanized on day 16, and the tissues were processed for histological and flow cytometry analyses ($n = 5$ mice). (**A**) Average spleen weight. (**B**) Histopathological analyses of spleen and liver tissues. Red boxes and yellow arrows show the tissue damage. Scale bars, 100 μm. (**C**) Representative flow cytometry plots of $CD8^+$ T cells in spleen. The frequencies of effector memory $CD8^+$ T cells ($T_{EM}$; $CD44^{high}CD62L^{low}$) among $CD8^+$ T cells are shown. (**D**) Counts of $T_{EM}$ in spleen. (**E**) Counts of $CD69^+CD8^+$ T cells in spleen. (**F**) Counts of GrzmB-secreting $CD8^+$ T cells ($GrzmB^+CD8^+$) in spleen. (**G**) Representative flow cytometry plots of liver-infiltrating $CD8^+$ T cells. The frequencies of $CD8^+$ T cells among liver-infiltrating lymphocytes ($CD45.2^+$) are shown. (**H**) Counts of liver-infiltrating $CD8^+$ T cells. (**I**) Counts of liver-infiltrating $CD69^+CD8^+$ T cells. (**J**) Counts of liver-infiltrating GrzmB-secreting $CD8^+$ T cells. (**K**) Serum activity of alanine aminotransferase (ALT). (**L**) Serum concentration of IFN-γ. All data represent the mean ± SEM and are analyzed by one-way ANOVA.

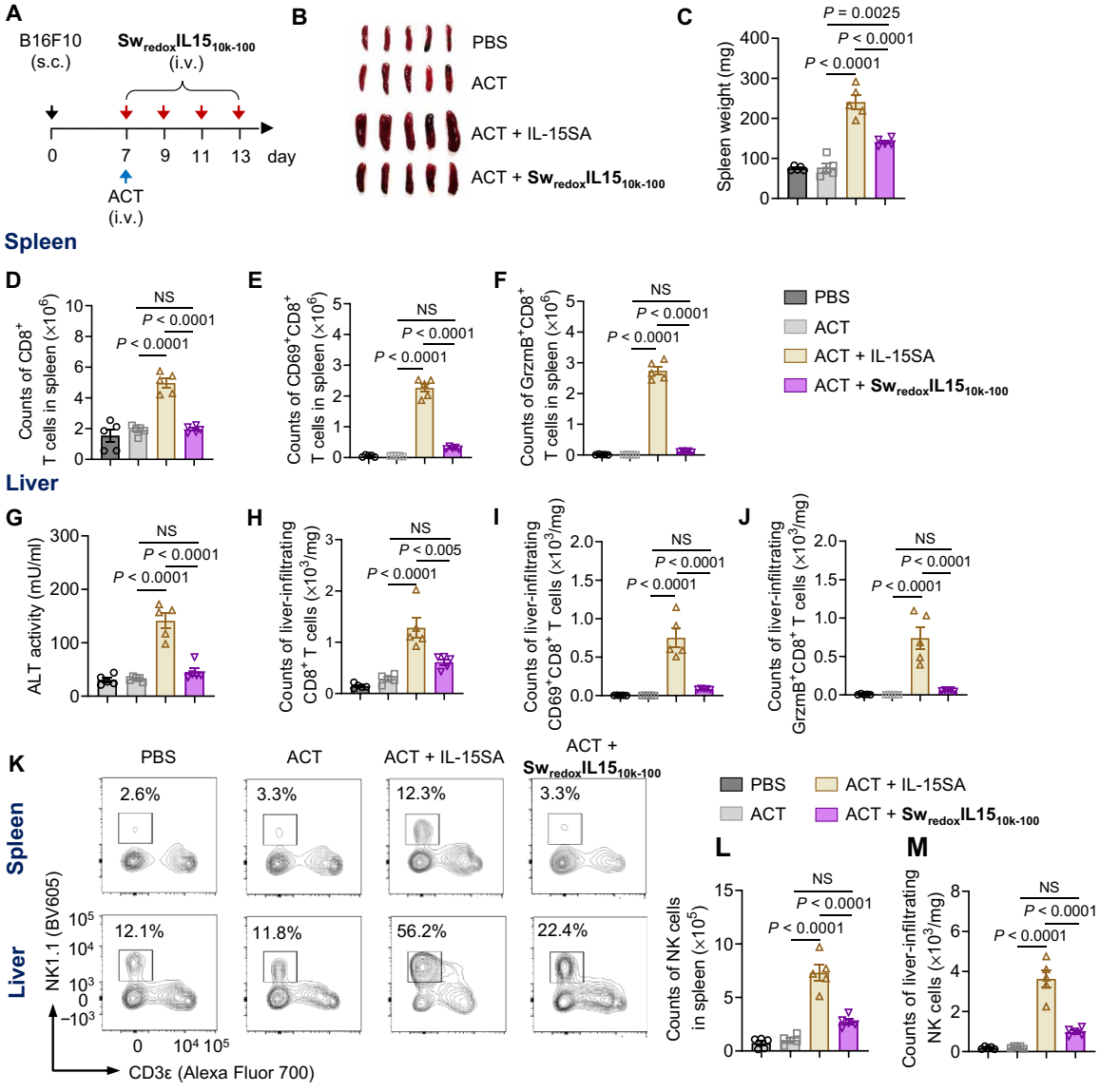


**Fig. 5. Sw-IM markedly reduced the toxicity of the combinational immunotherapy of IL-15SA and ACT.** (**A**) C57BL/6 mice were inoculated subcutaneously with B16F10 melanoma cells ($5 \times 10^5$) and received adoptive transfer of Thy1.1$^+$CD8$^+$ T cells ($1 \times 10^7$) on day 7 followed by intravenous administration of native IL-15SA (10 μg), Sw$_{redox}$IL15$_{10k-100}$ (equivalent dose of IL-15SA), or PBS every other day from days 7 to 13. Mice were euthanized on day 14, and the tissues were processed for flow cytometry analyses ($n = 5$ mice). (**B**) Images of excised spleens showing the splenomegaly. (**C**) Average spleen weight. (**D**) Counts of CD8$^+$ T cells in spleen. (**E**) Counts of CD69$^+$CD8$^+$ T cells in spleen. (**F**) Counts of GrzmB-secreting CD8$^+$ T cells in spleen. (**G**) Serum activity of ALT. (**H**) Counts of liver-infiltrating CD8$^+$ T cells. (**I**) Counts of liver-infiltrating CD69$^+$CD8$^+$ T cells. (**J**) Counts of liver-infiltrating GrzmB-secreting CD8$^+$ T cells. (**K**) Representative flow cytometry plots of NK cells in spleen (top) and liver (bottom). (**L**) Counts of NK cells in spleen. (**M**) Counts of liver-infiltrating NK cells. All data represent the mean ± SEM and are analyzed by one-way ANOVA.

(CD8$^+$ T cells and NK cells) as well as the activated and cytotoxic CD8$^+$ T cell subsets were maintained at the same level as that in the ACT alone group. In the therapeutic setting with prior lymphodepletion, the treatment with Sw$_{redox}$IL15$_{10k-75}$ (table S1, entry 35) at equivalent or even fourfold higher dose of the native IL-15SA induced greatly reduced spleen and liver toxicities (fig. S15). Together, Sw-IMs markedly improved the safety of mono- and combinational immunotherapies.

## Investigating the optimum formulation of Sw-IMs

The formulation parameters of Sw-IMs play a crucial role in their antitumor activity and safety profile. To quickly determine the optimum formulation for a given IM, we used the in vitro T cell activation assay for screening various formulations. The MFI of CD69 was used as a representative indicator for antitumor activity (on status) and toxicity (off status). We prepared a small library of 15 different formulations of Sw$_{redox}$IL15s (fig. S16A). As expected, both $R_C$ and $M_{PEG}$ influenced the CD69 MFI for Sw$_{redox}$IL15s at on or off status (fig. S16, B and C).

To better compare the overall performance of Sw-IMs of various formulations, we defined a comprehensive performance index, $E_S$, which was the ratio of CD69 MFI for Sw$_{redox}$IL15s at on status to that at off status (Fig. 6A). The higher $E_S$ value suggests enhanced overall performance of Sw-IM with potentially increased antitumor activity as well as reduced toxicity in healthy tissues. The native

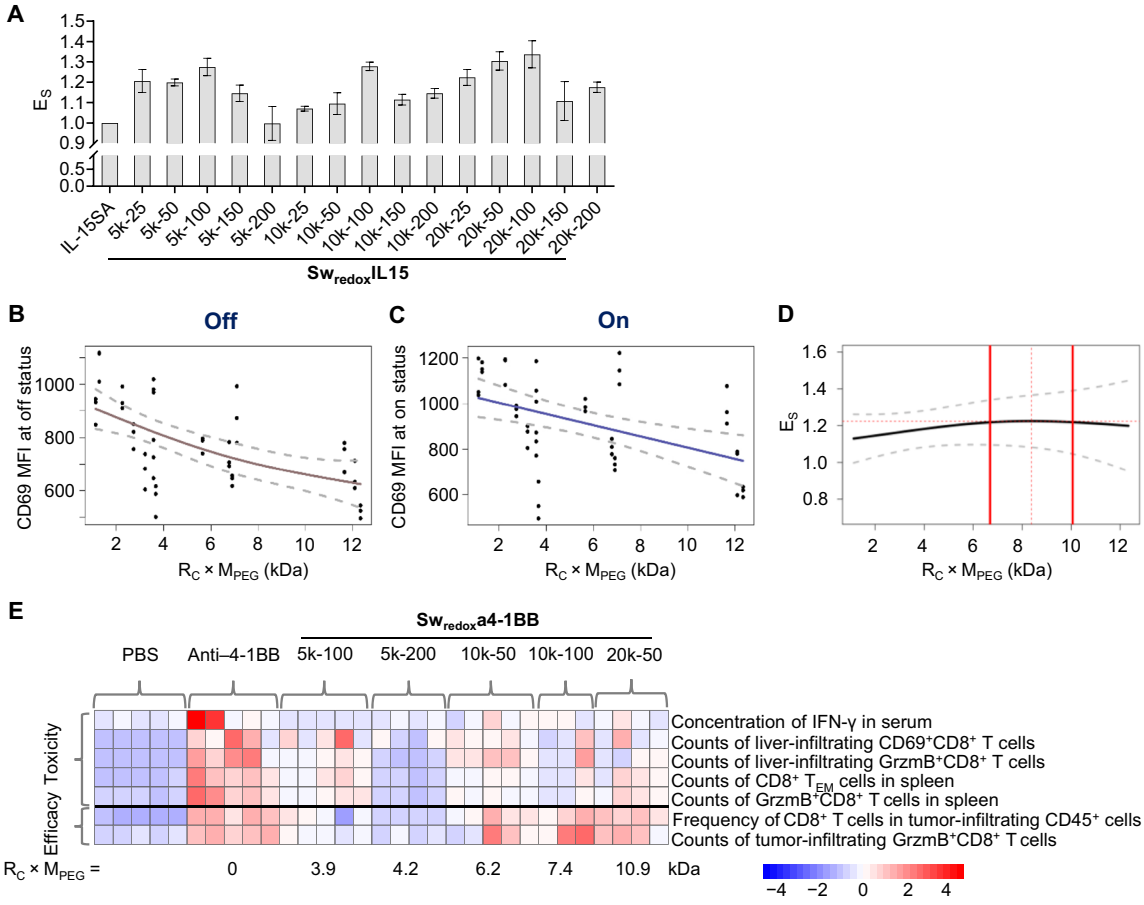


**Fig. 6. Investigation of the optimum formulation parameters of Sw-IMs.** (**A**) Comprehensive performance index ($E_S$) of $Sw_{redox}$IL15s of different formulations. $E_S$ = CD69 MFI at on status/CD69 MFI at off status. (**B** and **C**) Plots of CD69 MFI of $CD8^+$ T cells cultured with $Sw_{redox}$IL15s at off and on status as a function of the comprehensive formulation index $R_C \times M_{PEG}$. (**D**) Plot of $E_S$ as a function of $R_C \times M_{PEG}$. Gray dashed lines indicate 95% prediction intervals (B to D). Red dashed line indicates the peak value. Thick red lines indicate optimal range defined as 30% of the range of data on the *x* axis, centered on the peak value. (**E**) Heatmap illustrating the average of the indicated parameters for in vivo toxicity (above the black line) and therapeutic efficacy (below the black line). Rows represent averaged *z* scores. Each column represents a treated mouse receiving the indicated treatment.

IL-15SA has an $E_S$ value of 1 as there is no difference of its activities in various tissues. In addition, we defined a comprehensive formulation index, $R_C \times M_{PEG}$, representing the overall masking effect of conjugated polymers. The smooth fit to CD69 MFI values at off status as a function of $R_C \times M_{PEG}$ via penalized cubic regression splines showed a concave curve with higher slope at low $R_C \times M_{PEG}$, while the plot of CD69 MFI at on status showed a near-linear curve (Fig. 6, B and C). As a result, the plot of $E_S$ as a function of $R_C \times M_{PEG}$ shows a convex curve with a peak in the range of $R_C \times M_{PEG}$ = 6.7 to 10.1 kDa, suggesting an optimal range of the formulation index (Fig. 6D). These observations correlated well with the in vivo results of Sw-IMs. Among the $Sw_{redox}$a4-1BBs tested in vivo (Fig. 6E), $Sw_{redox}$a4-1$BB_{10k\text{-}100}$ with an $R_C \times M_{PEG}$ value of 7.4 kDa showed the highest antitumor efficacy and the least toxicity; $Sw_{redox}$a4-1$BB_{10k\text{-}50}$ and $Sw_{redox}$a4-1$BB_{20k\text{-}50}$ with $R_C \times M_{PEG}$ values of 6.2 and 10.9 kDa, respectively, also exhibited high antitumor efficacy but slightly increased toxicity compared to $Sw_{redox}$a4-1$BB_{10k\text{-}100}$.

## DISCUSSION

IM therapeutics that stimulate anticancer immunity may result in systemic toxicities because of nonspecific immune activation in the circulation or healthy tissues, greatly limiting their therapeutic potential in the clinic. Here, we demonstrated a responsive chemical masking strategy, termed Sw-IM, to achieve tumor-specific activation of the IMs. Sw-IMs applied to antibody- or cytokine-based immunotherapeutics markedly reduced the immunotoxicity while retaining their therapeutic potency, leading to prolonged survival of tumor-bearing mice.

The Sw-IM approach is highly versatile and modular. We have applied the syntheses to the preparation of 58 different Sw-IMs in total (Table 1 and table S1). Each Sw-IM consists of three modular parts: a protein-based therapeutic, a responsive linker, and a biocompatible polymer for reversible masking. We focused on a costimulatory agonist antibody, anti–4-1BB antibody, and a cytokine superagonist, IL-15SA, to prove the concept in mouse tumor models, because these two IMs have been shown to not only have potent antitumor activities but also exhibit severe immune-related adverse effects in preclinical and clinical studies (*1*, *3*, *42*, *43*). This approach was also successfully extended to checkpoint blockade antibodies including anti–PD-1 and anti–CTLA-4 antibodies. Any biomacromolecule agents bearing multiple functional groups (e.g., amino groups) could potentially be formulated into Sw-IM. Sw-IMs can be

rendered with different responsiveness using diverse trigger-degradable linkers. The TME is characterized as being reducing, acidic, hypoxic, and overexpressing various proteases among other signatures (*44*). Implementation of responsive chemistry that has been developed for drug delivery applications in addition to the redox and acidic pH–responsive linkers could further expand the library of Sw-IMs. Other natural or synthetic polymers besides PEG that are hydrophilic, biocompatible, and with low immunogenicity could also be used as masking polymers for Sw-IMs.

The high modularity of the Sw-IM enabled us to fine-tune the formulations for the optimized antitumor efficacy and safety profile. An optimal Sw-IM should exhibit the minimum activities in blood circulation and healthy tissues (off status) but the maximum activities in the TME (on status). Given a biomacromolecule therapeutic and a responsive linker, the performance of Sw-IM is determined by the overall masking effect of the conjugated polymers. We thus defined a comprehensive formulation index, $R_C \times M_{PEG}$, which is proportional to the average total mass of polymer mask. The activity of Sw-IM at off status drops rapidly as $R_C \times M_{PEG}$ increases (especially, when $R_C \times M_{PEG} < 6$ kDa) because the steric hindrance on binding between Sw-IM and its corresponding cellular receptor is augmented with increasing masking effect (Fig. 6B). One can speculate that the curve would eventually reach a constant minimum as the slope continuously declines, implying that the maximum hindrance would be achieved when the masking effect reaches saturation (Fig. 6B). Increasing masking effect also decreases the accessibility of reducing agents to the responsive linker, resulting in almost linearly declined activities of Sw-IM at on status (Fig. 6C). The peak in the plot of $E_S$ as a function of $R_C \times M_{PEG}$ implies that the optimal range of masking effect indeed exists. When the $R_C \times M_{PEG}$ value is too low (<6.7 kDa), Sw-IM exhibits relatively high toxicity profile because of insufficient masking (Fig. 6D). On the other hand, when the $R_C \times M_{PEG}$ value is too high (>10.1 kDa), Sw-IM may hardly regain any biological activities because of the inaccessibility of the reducing agent to the linker and thus may have low efficacy and low toxicity. Therefore, we need to optimize the formulation parameters for each Sw-IM with a suitable degree of masking for the balanced potency and safety.

This chemical strategy complements the recombinant approaches to target the IM activities specifically to the TME. Strategies using customized masking peptides (*19*), proteins (*22*, *23*), or a generalizable coiled-coil domain (*20*) for the preparation of recombinant antibody prodrug, termed "probody," are being actively pursued. Probody immunotherapy targeting ligand of programmed death 1 (PD-L1) is currently tested in the clinic (ClinicalTrials.gov, identifier: NCT03013491) (*45*, *46*). However, this probody design relies exclusively on the overexpressed proteases in the TME for triggered removal of masking peptides. The chemical modification with masking polymers presented here may allow much more diverse choices of responsiveness, therapeutics, and masking polymers. Besides the redox and acidic pH–responsive chemistry described above, other environment responsive chemistries, such as those responsive to matrix metalloproteinases (*47*), reactive oxygen species (*48*), or even external signals (*49*, *50*), can be potentially adapted to the syntheses of Sw-IMs. Recent reports of a hypoxia-activated conditional aptamer-PEG conjugate (*51*) and an antibody against hemagglutinin masked by a bivalent peptide-DNA ligand (*52*) provide the hint that the chemical approach can be further extended to nonprotein therapeutics or imaging probes.

## MATERIALS AND METHODS

### Materials

The monoclonal antibodies including anti–4-1BB (anti-CD137, clone 3H3), anti–PD-1 (clone 29F.1A12), anti–CTLA-4 (anti-CD152, clone 9H10), rat IgG2a isotype control (anti-TNP, clone 2A3), and anti-CD3 (clone 17A2) were purchased from Bio X Cell (West Lebanon, NH, USA). Methoxy PEG amine (mPEG-$NH_2$) with various MWs, methoxy PEG thiol (mPEG-SH), and methoxy PEG–DBCO (mPEG-DBCO) were purchased from JenKem Technology (Plano, TX, USA). Alexa Fluor 647 succinimidyl ester was purchased from Invitrogen (now Thermo Fisher Scientific, Waltham, MA, USA). Benzoyl peroxide [BPO; containing 25% (w/w) water as stabilizer, CAS 94-36-0] was purchased from Alfa Aesar (Ward Hill, MA, USA) and recrystallized twice with chloroform and methanol before use. 2-Hydroxyethyl disulfide (technical grade, CAS 1892-29-1), phosgene [15% (w/w) in toluene, CAS 75-44-5], trimethylamine (TEA; 99.5%, CAS 121-44-8), NHS (98%, CAS 6066-82-6), dimethylmaleic anhydride (DMMA; 98%, CAS 766-39-2), *N*-bromosuccinimide (NBS; 99%, CAS 128-08-5), TNBSA [5% (w/v) in $H_2O$, CAS 2508-19-2], SDS (20% in $H_2O$, CAS 151-21-3), reduced L-GSH (98%, CAS 70-18-8), and other chemicals were purchased from Sigma-Aldrich (St. Louis, MO, USA). Unless otherwise noted, all chemicals and reagents were used as received.

### Mice

Six- to 8-week-old female Thy1.2$^+$ C57BL/6 mice were purchased from Charles River Laboratories (Lyon, France). T cell receptor (TCR)–transgenic Thy1.1$^+$ pmel-1 (Pmel) mice [B6.Cg-*Thy1*$^a$/Cy Tg(TcraTcrb)8Rest/J] were originally purchased from The Jackson Laboratory (Bar Harbor, ME, USA) and maintained in École Polytechnique Fédérale de Lausanne (EPFL) animal core facility [Center of Phenogenomics (CPG)].

### Cell lines

The MC38 murine colon adenocarcinoma cell line was provided by D. J. Irvine's laboratory (MIT, MA, USA). B16F10 murine melanoma cells were originally acquired from the American Type Culture Collection (Manassas, VA, USA). The tumor cells were cultured in Dulbecco's modified Eagle's medium (Gibco/Thermo Fisher Scientific) supplemented with fetal bovine serum [FBS; 10% (v/v), Gibco/Thermo Fisher Scientific] and penicillin/streptomycin [1% (v/v), Gibco/Thermo Fisher Scientific].

### Production of mouse IL-15SA

The engineered IL-15SA construct (gWIZ-mIL-15SA) was a gift from D. J. Irvine (MIT). IL-15SA contains a mouse IL-15 fused at the C terminus of Sushi domain of a mouse IL-15Rα, which is next fused at the C terminus with a mouse IgG2c Fc. IL-15SA was expressed by human embryonic kidney (HEK) 293-E cells in Freestyle medium (Gibco) at the EPFL Protein Expression Core Facility (PECF). The supernatant of culture medium containing IL-15SA was harvested by centrifugation after a 7-day culture and was filtered through a filter membrane (0.22 μm) to obtain a clear solution. IL-15SA was first captured with a HiTrap Protein A affinity chromatography column on an ÄKTA pure 25 system (GE Healthcare, Chicago, IL, USA) and eluted with an elution buffer (0.05 M sodium citrate, 0.3 M sodium chloride, pH 3.0). The eluted protein was next collected immediately in a neutralization buffer (1 M tris-HCl, pH 10.0) followed by concentration with membrane ultrafiltration

(MW cutoff, 10 kDa) in Vivaspin (GE Healthcare). The concentrated protein solution was further purified with a Superdex 200 increase size exclusion column (GE Healthcare) at a flow rate of 1.0 ml/min with PBS buffer on an ÄKTA pure 25 system. The purity and activity of IL-15SA were confirmed with SDS-PAGE and T cell proliferation assay, respectively. The purified protein was aliquoted and stored at −80°C before use.

### Synthesis of redox-responsive linker NHS-SS-NHS

NHS-SS-NHS was prepared following a previous report (*53*). Briefly, in a 100-ml round-bottom flask, 2-hydroxyethyl disulfide (1.329 g, 8.616 mmol) in anhydrous tetrahydrofuran (20 ml) solution was added dropwise to a phosgene solution [12.5 ml, 15% (w/w), 18.95 mmol] in toluene. The reaction mixture was protected with $N_2$ and stirred under room temperature for 2 hours. The obtained solution was concentrated under vacuum, and the residue was dissolved with anhydrous dichloromethane (DCM; 10 ml) followed by addition of NHS (2.182 g, 18.95 mmol) and anhydrous TEA (1.918 g, 18.95 mmol) in DCM solution (45 ml). The reaction mixture was protected with $N_2$ and stirred at room temperature overnight and then concentrated under vacuum. The crude product was purified with column chromatography (DCM:methanol, 10:1) and recrystallized with icy petroleum ether. The acicular crystal (2.14 g, yield: 57%) was dried under vacuum and characterized by $^1$H nuclear magnetic resonance (NMR) (Bruker AVANCE NEO 400 MHz spectrometer, Billerica, MA, USA). $^1$H NMR (400 MHz, $CDCl_3$,): δ (ppm) = 4.61 (t, $J$ = 4 Hz, 4H, C$H_2$O), 3.08 (t, $J$ = 4 Hz, 4H, C$H_2$S), 2.88 (s, 8H, C$H_2$C$H_2$).

### Preparation of redox-responsive Sw-IMs

In the preparation of $Sw_{redox}$a4-1$BB_{10k\text{-}100}$, for example, mPEG-$NH_2$ in anhydrous dimethyl sulfoxide (DMSO) solution (133.3 nmol, 20 mg/ml, 1.0 equiv) was mixed with an NHS-SS-NHS solution (133.3 nmol, 40 mg/ml in anhydrous DMSO, 1.0 equiv). The reaction mixture was shaken in ThermoMixer (Eppendorf, Hamburg, Germany) at room temperature for 4 hours (800 rpm). The intermediate product was next added into an IM solution (1.33 nmol, 1 mg/ml in 0.1 M $NaHCO_3$, pH 8.5) for another hour of shaking. For other formulations, different feeding mole ratios ($R_F$) of PEG to IM were chosen. The crude product was purified by ultrafiltration (7500 rpm, 5 min × 5) in an Amicon centrifugal filter (MW cutoff, 50 kDa; Merck Millipore, Burlington, MA, USA). The concentration of the purified Sw-IM was determined with a NanoDrop microvolume ultraviolet-visible (UV-vis) spectrophotometer (Thermo Fisher Scientific). For the preparation of fluorescently labeled Sw-IMs, Alexa Fluor 647 succinimidyl ester (2.67 nmol, 10 mg/ml in anhydrous DMSO, 2.0 equiv) was added to a solution of IM (1.33 nmol, 1 mg/ml in 0.1 M $NaHCO_3$ buffer, pH 8.5, 1.0 equiv) followed by shaking in ThermoMixer for 20 min before the addition of the PEG intermediate product.

### Switch on of redox-responsive Sw-IMs

A solution of Sw-IM in PBS (pH 7.4, 1 mg/ml, 50 μl) was mixed with a solution of L-GSH in PBS (10 mM, pH 7.4, 50 μl). The mixed solution was incubated at room temperature for 1 hour and purified by ultrafiltration (MW cutoff, 50 kDa; 7500 rpm; 5 min × 2) in an Amicon centrifugal filter to get rid of any small molecules and the released mPEG-$NH_2$. The concentration of recovered IMs was determined by a NanoDrop UV-vis spectrophotometer. Released IMs were analyzed by SDS-PAGE, TNBSA, and flow cytometry assays.

### Synthesis of (bromomethyl)methylmaleic anhydride

BrMMMA [(bromomethyl)methylmaleic anhydride] was prepared following a previous report (*54*). Briefly, recrystallized BPO (200 mg, 0.83 mmol, 0.017 equiv) was added into the mixture of DMMA (5.04 g, 50 mmol, 1.0 equiv) and NBS (14.24 g, 100 mmol, 2.0 equiv) in carbon tetrachloride in a 500-ml round-bottom flask. The suspension was refluxed for 5 hours. After cooling down to room temperature, a second portion of BPO (200 mg, 0.83 mmol, 0.017 equiv) was added to the reaction mixture followed by another 5-hour reflux. The reaction was then cooled down to room temperature and kept stirring overnight. The suspension was filtered to get rid of any insoluble impurities and washed with water (100 ml × 2) and brine (100 ml × 2). The organic layer was then dried with anhydrous $Na_2SO_4$ and concentrated under vacuum. The obtained crude product as sticky yellow oil was purified by column chromatography (EtOAc:petroleum ether, 4:1) and further distilled with a Kugelrohr apparatus (90°C, 0.005 mbar). The second fraction as light yellow oil was collected as pure product (4.0 g, yield 60%). $^1$H NMR (400 MHz, $CDCl_3$): δ (ppm) = 4.20 (s, 2H, C$H_2$Br), 2.19 (s, 3H, C$H_3$).

### Synthesis of AzMMMA

AzMMMA was prepared following a previous report (*55*). Briefly, sodium azide (130 mg, 2.0 mmol, 1.0 equiv) was added rapidly to an acetone solution (20 ml) of BrMMMA (410 mg, 2.0 mmol, 1.0 equiv) in a 50-ml round-bottom flask. The mixture was vigorously stirred at room temperature overnight to generate a purple suspension. The reaction mixture was then filtered to get rid of solid residues and then concentrated under vacuum. The obtained sticky oil was diluted with ethyl acetate (50 ml) and washed with water (50 ml × 2) and brine (50 ml × 2). The organic layer was then collected and dried with anhydrous $Na_2SO_4$. After being concentrated under vacuum, the crude product was purified by column chromatography (ethyl acetate:petroleum ether, 2:1) to provide the pure product as colorless oil (270 mg, yield 80%). $^1$H NMR (400 MHz, $CDCl_3$): δ (ppm) = 4.29 (d, $J$ < 1.0 Hz, 2H, C$H_2$N$_3$), 2.23 (t, $J$ = 1.0 Hz, 3H, C$H_3$).

### Preparation of $Sw_{pH(D)}$a4-1BB

In the preparation of $Sw_{pH(D)}$a4-1$BB_{5k\text{-}400}$, for example, to a basic buffer solution (0.1 M $NaHCO_3$, pH 8.5) of anti–4-1BB (200 μg, 1.33 nmol, 2 mg/ml), AzMMMA (20 mg/ml in anhydrous DMSO, 4.45 μl, 0.53 μmol, 400 equiv) was added. The reaction mixture was shaken in ThermoMixer at room temperature for 2 hours. The mixture was washed via ultrafiltration (MW cutoff, 50 kDa; 7500 rpm; 5 min × 5) in an Amicon centrifugal filter to remove the unreacted AzMMMA. The purified azido-functionalized antibodies were then diluted with basic buffer to a concentration of 1 mg/ml and added to a solution of mPEG-DBCO (MW = 5 kDa, 25 mg/ml in basic buffer, 400 equiv). The reaction mixture was shaken for another 2 hours (800 rpm, room temperature) and purified by ultrafiltration similarly.

### Synthesis of MMMA functionalized PEG

mPEG-SH (MW = 5 kDa, 300 mg, 0.06 mmol) was dissolved in methanol (2 ml) in a 5-ml round-bottom flask. The solution was purged with $N_2$ for 10 min to eliminate $O_2$. KOH (6.7 mg, 0.12 mmol) in methanol solution (1 ml) was then added dropwise over 10 min to the mPEG-SH solution with vigorous stirring. The mixed solution was cooled down to 0°C in an ice-salt bath and added with

BrMMMA (25 mg) in methanol solution (2 ml) dropwise over 10 min. The reaction mixture was then stirred at 0°C for 30 min followed by concentration under vacuum. The residues were redissolved in dilute hydrogen chloride (HCl) solution (1 M, 5 ml). After stirring at room temperature for another 2 hours, the aqueous solution was saturated with NaCl and extracted with DCM. The organic layer was combined and dried with anhydrous $Na_2SO_4$, and concentrated under vacuum to provide the product as white powder (230 mg, yield 77%). $^1$H NMR (400 MHz, $CDCl_3$): δ (ppm) = 3.67 (s, C$H_2$-C$H_2$), 2.19 (s, C$H_3$), 2.78 (s, C$H_2$).

### Preparation of $Sw_{pH(S)}$a4-1BBs

In the preparation of $Sw_{pH(S)}a4\text{-}1BB_{5k\text{-}400}$, for example, powder of mPEG-MMMA (MW = 5 kDa, 2.67 mg, 0.53 μmol, 400 equiv) was added to the native anti–4-1BB (200 μg, 1.33 nmol, 1 mg/ml) in a basic buffer (PBS + $Na_2CO_3$, pH 9.5). The reaction mixture was shaken in ThermoMixer at room temperature for 4 hours and then purified by ultrafiltration (MW cutoff, 50 kDa; 7500 rpm; 5 min × 5) with an Amicon centrifugal filter.

### Switch on of acidic pH–responsive Sw-IMs

Solution of acidic pH–responsive Sw-IMs was transferred to an acidic phosphate buffer (pH 6.5) by ultrafiltration (MW cutoff, 50 kDa) with an Amicon centrifugal filter and diluted to the concentration of 1 mg/ml. The solution was incubated at 37°C overnight. The recovered antibodies were then transferred back to neutral PBS (pH 7.4) via ultrafiltration (MW cutoff, 50 kDa) for SDS-PAGE, TNBSA, and flow cytometry assays.

### SDS-PAGE gel electrophoresis

The PBS solution of native IMs and Sw-IMs at off and on status (0.5 mg/ml, 15 μl, pH 7.4) was mixed with Bolt LDS sample buffer (4×, 5 μl; Life Technologies, Carlsbad, CA, USA) and added into the well of a NuPAGE 4 to 12% bis-tris gel (1.0 mm × 12 wells; Novex/Thermo Fisher Scientific). The samples were separated in Mops SDS running buffer (Novex/Thermo Fisher Scientific) at 110 V for 1 hour. The collected gel was then stained with Coomassie Brilliant Blue staining buffer [0.25% (w/v) in 45% MeOH, 45% $H_2O$, and 10% acetic acid] for 1 hour followed by washing with destaining solution (10% acetic acid, 30% EtOH, and 60% $H_2O$). The gels were recorded with an E-Gel Imager system (Thermo Fisher Scientific).

### UHPLC-SEC characterization

Native IMs and Sw-IMs were diluted by filtered PBS (pH 7.4) to 1 mg/ml. A mobile phase of PBS (containing 200 mM NaCl, pH 7.4) was applied on an UltiMate 3000 UHPLC system equipped with a BioBasic SEC 300 LC column (Thermo Fisher Scientific) with a flow rate of 0.5 ml/min. The traces were monitored with a diode array detector (UV, Dionex UltiMate 3000, Thermo Fisher Scientific) and a fluorescence detector (FLD, Dionex UltiMate 3000, Thermo Fisher Scientific).

### DLS characterization

Native IMs and Sw-IMs were diluted with filtered PBS (pH 7.4) to 0.1 mg/ml and transferred into PS semi-micro cuvettes (Brand, Wertheim am Main, Germany). The diameter of the product was measured with a NanoZS (Marven, Worcester, UK) DLS instrument at room temperature. The measurement was repeated three times independently for each sample.

### Conjugation ratio determined by TNBSA assay

Solutions of native IMs and Sw-IM at off or on status (100 μl, 200 μg/ml in $NaHCO_3$ buffer, pH 8.5) or a small-molecule standard, 5-amino-1-pentanol (100 μl, gradient diluted from 20 μg/ml in $NaHCO_3$ buffer, pH 8.5), were mixed with a solution of TNBSA [50 μl, 0.1% (w/v) in $NaHCO_3$ buffer, pH 8.5] in a flat-bottom 96-well plate. The reaction mixture was incubated at 37°C for 2 hours. A solution of SDS [50 μl, 10% (w/v) in $H_2O$] was added to each well followed by addition of HCl solution (25 μl, 1 N in $H_2O$) to stop the reaction. The UV absorbance at the wavelength of 335 nm was measured with a Varioskan LUX microplate reader (Thermo Fisher Scientific). The concentration of primary amines was calculated using the calibration curve of 5-amino-1-pentanol standard.

### Preparation of activated Pmel $CD8^+$ T cells

Spleens from Pmel mice were mechanically disrupted into individual cells by smashing on a 70-μm strainer (Fisher Scientific, Pittsburgh, PA, USA) and then lysed with ACK lysing buffer (2 ml per spleen, Gibco/Thermo Fisher Scientific) for 5 min to get rid of the red blood cells. The cells were then washed with PBS and resuspended to a cell density of around $1.0 \times 10^6$/ml with complete RPMI 1640 culture medium (Gibco/Thermo Fisher Scientific) containing FBS (10%, v/v), Hepes (1%, v/v), penicillin/streptomycin (1%, v/v), and β-mercaptoethanol (0.1%, v/v), supplemented with mouse IL-2 (10 ng/ml; PeproTech, London, UK), IL-7 (2 ng/ml; PeproTech), and $gp100_{25–33}$ (1 μM; GenScript, Piscataway, NJ, USA). After culturing for 3 days at 37°C with 5% $CO_2$, the live cells were enriched by density gradient centrifugation with Ficoll-Paque PLUS (GE Healthcare). The collected cells were cultured for extra 2 days with a cell density of around $1.0 \times 10^6$/ml in complete RPMI medium supplemented with mouse IL-2 (10 ng/ml) and IL-7 (2 ng/ml) before use.

### In vitro T cell binding assay

Activated Pmel $CD8^+$ T cells ($1 \times 10^5$) in each well of a U-bottom 96-well plate were blocked with anti-CD16/32 antibodies and stained with anti-CD8β. After washing twice with flow cytometry buffer [PBS containing bovine serum albumin, 0.2% (w/v)], the cells were resuspended with series diluted fluorescently labeled IM solutions (133.3 to 1.7 pM for anti–4-1BB and anti–PD-1, and 222.2 to 2.8 pM for IL-15SA, 100 μl for each well) or fluorescently labeled Sw-IM solutions (equivalent mole concentration to native IM) in flow cytometry buffer and incubated at 4°C for 1 hour. After washing twice with flow cytometry buffer (200 μl), the cells were stained with 4′,6-diamidino-2-phenylindole (DAPI; Sigma-Aldrich) for flow cytometry analysis.

### In vitro T cell activation assay for $Sw_{redox}$IL15

Activated Pmel $CD8^+$ T cells were washed twice with PBS (200 μl) to remove the trace cytokines in the culture medium. The cells were resuspended with the solutions of native IL-15SA (2.2 nM to 0.18 pM, 100 μl for each well) or $Sw_{redox}$IL15s (equivalent mole concentration to native IL-15SA, at either off or on status) in complete RPMI 1640 culture medium in a U-bottom 96-well plate ($1 \times 10^5$ cells for each well). The cells were cultured at 37°C for 48 hours and then stained for flow cytometry analysis. For the investigation on optimal formulations, the applied concentration is 0.55 nM for native IL-15SA and equivalent mole concentration for $Sw_{redox}$IL15s.

### In vitro T cell activation assay for $Sw_{redox}$a4-1BB

Spleens from Pmel mice were mechanically disrupted and lysed with ACK lysing buffer as described above. After washing with PBS, naïve $CD8^+$ T cells were isolated using the $CD8^+$ T Cell Isolation Kit (Miltenyi Biotec, North Rhine-Westphalia, Germany) following the manufacturer's protocol. Briefly, cells were resuspended in PBS (200 μl) and added with CD8 (TIL) MicroBeads (20 μl). After incubating at 2° to 8°C for 15 min, the cell suspension was passed over a MACS Column using the MACS Separator for positive selection. The fraction of purified $CD8^+$ T cells was resuspended in complete RPMI 1640 culture medium containing FBS (10% v/v), Hepes (1% v/v), penicillin/streptomycin (1% v/v), and β-mercaptoethanol (0.1% v/v) at cell density of $2.0 \times 10^6$/ml.

U-bottom 96-well plates were first coated with anti-CD3 antibody by incubating with the PBS solution of anti-CD3 (0.1 μg/ml, 100 μl) overnight at 4°C. The supernatant was then discarded, and each well was loaded with naïve $CD8^+$ T cells ($2 \times 10^5$ per well) suspended in complete RPMI culture medium. Next, the solution of native anti–4-1BB (133.3 to 0.013 nM, 10-fold gradient dilution) and $Sw_{redox}$a4-1BBs (equivalent mole concentration with native anti–4-1BB) in complete RPMI culture medium (100 μl) was added on top of each well. The cells were incubated at 37°C for 48 hours and stained for flow cytometry analysis.

### Flow cytometry analyses

For surface marker staining, cells in a U-bottom 96-well plate were blocked with anti-CD16/32 antibodies and then stained with indicated antibodies at 4°C for 20 min followed by LIVE/DEAD staining with DAPI or Zombie Aqua Fixable Dye (BioLegend, San Diego, CA, USA). After washing with flow cytometry buffer (200 μl), the cells were resuspended with the same buffer (200 μl) for flow cytometry analysis.

For intracellular cytokine staining, the cells were first stimulated with the Cell Stimulation Cocktail (protein transport inhibitors included, Invitrogen/Thermo Fisher Scientific) at 37°C for 6 hours. The surface marker staining and LIVE/DEAD staining with Zombie Aqua Fixable Dye was then performed as described above. The cells were then fixed with a Cytofix/Cytoperm Fixation/Permeabilization solution (BD Biosciences, Franklin Lakes, NJ, USA) and incubated with indicated antibodies against cytokines at 4°C for 30 min. The stained cells were resuspended in flow cytometry buffer (200 μl) for flow cytometry analyses.

All flow cytometry data were collected with an Attune NxT flow cytometer (Invitrogen/Thermo Fisher Scientific) and analyzed by FlowJo 10.6.1 (Tree Star, Ashland, OR, USA). Gate margins were determined by isotype controls and fluorescence-minus-one (FMO) controls.

### Antibodies for flow cytometry

The antibodies for flow cytometry analysis including anti-CD16/32 (clone 93), anti-CD3ε (clone 17A2), anti-CD8β (clone 53-6.7), anti-CD44 (clone IM7), anti-CD62L (clone MEL-14), anti-CD19 (clone 6D5), anti-CD45.2 (clone 104), anti-CD4 (clone RM4-5), anti-Thy1.1 (clone OX-7), anti-NK1.1 (clone PK136), anti-GrzmB (clone GB11), anti–IFN-γ (clone XMG1.2), anti–TNF-α (clone MP6-XT22), and anti–IL-2 (clone JES6-5H4) were purchased from BioLegend.

### Therapeutic and toxicity studies

In evaluating $Sw_{redox}$a4-1BBs as monotherapies, C57BL/6 mice were inoculated subcutaneously with MC38 cells ($2 \times 10^5$) on the right flank and received intraperitoneal injections of native anti–4-1BB (100 μg), $Sw_{redox}$a4-1BBs (equivalent dose of anti–4-1BB), or PBS on days 4, 7, and 10. Tumor growth was recorded as the volume of tumor ($^1/_2$ length × width$^2$), and the body weight of the mice was measured every other day starting from day 4. Mice were euthanized on day 16, and the tissues (tumor, liver, and spleen) were processed for histological and flow cytometry analyses ($n = 5$ mice).

In evaluating the combination therapy of ACT and $Sw_{redox}IL15_{10k\text{-}100}$, C57BL/6 mice were inoculated subcutaneously with B16F10 murine melanoma cells ($5 \times 10^5$) and received adoptive transfer of $Thy1.1^+CD8^+$ T cells ($1 \times 10^7$) on day 7 followed by intravenous injection of IL-15SA (5 μg for each injection), $Sw_{redox}IL15_{10k\text{-}100}$ (equivalent dose of IL-15SA), or PBS every other day starting from day 7 until day 21. The tumor volume and body weight were measured every other day. In a toxicity study, mice were treated similarly and euthanized on day 14 and the tissues (tumor, liver, and spleen) were processed for flow cytometry analyses. To evaluate the combination therapy with lymphodepletion, the tumor-bearing mice were irradiated under 4 Gy 1 day before adoptive transfer of $Thy1.1^+CD8^+$ T cells on day 7 and intravenous injection of native IL-15SA (10 μg for each injection), $Sw_{redox}IL15_{10k\text{-}100}$ (equivalent dose of IL-15SA), or PBS every other day from days 7 to 21. In toxicity study, the tumor-bearing mice were irradiated under 4 Gy 1 day before adoptive transfer of $Thy1.1^+CD8^+$ T cells on day 7 and intravenous injection of native IL-15SA, $Sw_{redox}IL15_{10k\text{-}75}$ (equivalent or four times dose of IL-15SA), or PBS on days 7, 9, and 11. The mice were euthanized on day 12, and the tissues were processed for flow cytometry analyses. In all studies, mice were euthanized when the body weight loss was >10% of the predosing weight or the tumor area reached 1000 mm$^3$ (as a predetermined end point).

### Tissue processing for flow cytometry analyses

After euthanasia, the spleen was collected and disrupted into single-cell suspension with a 70-μm cell strainer. Red blood cells were lysed with ACK lysis buffer at room temperature for 5 min. For liver- and tumor-infiltrating lymphocytes, one lobe of liver and the tumor was first digested with tumor digestion buffer [RPMI 1640 medium with collagenase type IV (1 mg/ml; Gibco/Thermo Fisher Scientific), dispase II (100 μg/ml, Sigma-Aldrich), hyaluronidase (100 μg/ml; Sigma-Aldrich), and deoxyribonuclease I (100 μg/ml; Sigma-Aldrich)] at 37°C for 1 hour. The remaining residue of liver and tumor tissue was next ground through a 70-μm cell strainer. After ACK lysis, live cells were enriched by density gradient centrifugation with a Percoll solution (40 and 80%, v/v) and then washed (10 ml) and resuspended in flow cytometry buffer (200 μl) for flow cytometry analyses.

### Histological study

Half of the spleen, one lobe of the liver, or part of the tumor was fixed in 4% paraformaldehyde overnight followed by imbedding in paraffin blocks. Paraffin slides were sectioned at a thickness of 4 μm and stained with hematoxylin and eosin (H&E) for pathological analysis at the EPFL Histology Core Facility (HCF). H&E images were captured with the DM5500 Upright Microscope (Leica, Wetzlar, Germany) at the EPFL BioImaging & Optics Platform (BIOP).

### Measurement of liver enzymes and cytokine concentration in serum

The whole blood (200 to 300 μl) was collected from inferior vena cava of the mice immediately after the euthanasia. The serum

samples were then prepared by centrifuging the whole blood in a Microvette 500 Z tube (Sarstedt, Nümbrecht, Germany). The activity of ALT in serum was measured using Stanbio Chemistry Reagents (Stanbio, Boerne, TX, USA) per the manufacturer's instructions. The concentration of IFN-γ was measured with an enzyme-linked immunosorbent assay (ELISA) kit (BD Biosciences).

### Scatterplot smoothing

In analyzing the results of comprehensive performance index $E_S$ of various formulations (Fig. 6, B to D), we used the penalized cubic regression splines as implemented in the mgcv R package (version 1.8-33) to fit smooth curves through scatterplots (*56*). To obtain the plot of in vitro comprehensive performance index $E_S$

$$E_S = \frac{\text{CD69 MFI on}}{\text{CD69 MFI off}}$$

as a function of $R_C$ or comprehensive formulation index $R_C \times M_{PEG}$, we separately fitted smooth curves for CD69 MFI at off and on status. We took the ratio of predicted fits to compute $E_S$ and used the chain rule to propagate the prediction intervals obtained for the numerator and the denominator to the $E_S$ ratio

$$\text{if } z = c\frac{x}{y} \text{ then } \frac{\delta z}{z} = \left[\left(\frac{\delta x}{x}\right)^2 + \left(\frac{\delta y}{y}\right)^2\right]^{0.5}$$

### Statistical analysis

Statistical analyses were performed using GraphPad Prism 8 (GraphPad Software Inc., La Jolla, CA, USA). Unless otherwise noted, the data are presented as mean ± SEM. Comparisons of survival curves were performed by the log-rank test. Comparisons of multiple groups at a single time point were performed by using one-way analysis of variance (ANOVA). For heatmap visualization, the efficacy and toxicity indictors were presented as *z* scores.

### Ethics statement

Experiments and handling of mice were conducted under federal, state, and local guidelines with approval from the Swiss authorities (Canton of Vaud, animal protocol IDs 3206 and 3533) and performed in accordance with the guidelines from CPG of EPFL.

## SUPPLEMENTARY MATERIALS

Supplementary material for this article is available at https://science.org/doi/10.1126/sciadv.abg7291

View/request a protocol for this paper from *Bio-protocol*.

## REFERENCES AND NOTES


1. N. H. Segal, T. F. Logan, F. S. Hodi, D. McDermott, I. Melero, O. Hamid, H. Schmidt, C. Robert, V. Chiarion-Sileni, P. A. Ascierto, M. Maio, W. J. Urba, T. C. Gangadhar, S. Suryawanshi, J. Neely, M. Jure-Kunkel, S. Krishnan, H. Kohrt, M. Sznol, R. Levy, Results from an integrated safety analysis of urelumab, an agonist anti-CD137 monoclonal antibody. *Clin. Cancer Res.* **23**, 1929–1936 (2017).
2. B. A. Baldo, Side effects of cytokines approved for therapy. *Drug Saf.* **37**, 921–943 (2014).
3. Y. Guo, L. Luan, W. Rabacal, J. K. Bohannon, B. A. Fensterheim, A. Hernandez, E. R. Sherwood, IL-15 superagonist-mediated immunotoxicity: Role of NK cells and IFN-γ. *J. Immunol.* **195**, 2353–2364 (2015).
4. C. Chester, M. F. Sanmamed, J. Wang, I. Melero, Immunotherapy targeting 4-1BB: Mechanistic rationale, clinical results, and future strategies. *Blood* **131**, 49–57 (2018).
5. C. A. Klebanoff, S. E. Finkelstein, D. R. Surman, M. K. Lichtman, L. Gattinoni, M. R. Theoret, N. Grewal, P. J. Spiess, P. A. Antony, D. C. Palmer, Y. Tagaya, S. A. Rosenberg, T. A. Waldmann, N. P. Restifo, IL-15 enhances the in vivo antitumor activity of tumor-reactive CD8+ T Cells. *Proc. Natl. Acad. Sci. U.S.A.* **101**, 1969–1974 (2004).
6. E. F. Zhu, S. A. Gai, C. F. Opel, B. H. Kwan, R. Surana, M. C. Mihm, M. J. Kauke, K. D. Moynihan, A. Angelini, R. T. Williams, M. T. Stephan, J. S. Kim, M. B. Yaffe, D. J. Irvine, L. M. Weiner, G. Dranoff, K. D. Wittrup, Synergistic innate and adaptive immune response to combination immunotherapy with anti-tumor antigen antibodies and extended serum half-life IL-2. *Cancer Cell* **27**, 489–501 (2015).
7. K. C. Conlon, E. Lugli, H. C. Welles, S. A. Rosenberg, A. T. Fojo, J. C. Morris, T. A. Fleisher, S. P. Dubois, L. P. Perera, D. M. Stewart, C. K. Goldman, B. R. Bryant, J. M. Decker, J. Chen, T. A. Worthy, W. D. Figg Sr., C. J. Peer, M. C. Sneller, H. C. Lane, J. L. Yovandich, S. P. Creekmore, M. Roederer, T. A. Waldmann, Redistribution, hyperproliferation, activation of natural killer cells and CD8 T cells, and cytokine production during first-in-human clinical trial of recombinant human interleukin-15 in patients with cancer. *J. Clin. Oncol.* **33**, 74–82 (2015).
8. L. Zhang, R. A. Morgan, J. D. Beane, Z. Zheng, M. E. Dudley, S. H. Kassim, A. V. Nahvi, L. T. Ngo, R. M. Sherry, G. Q. Phan, M. S. Hughes, U. S. Kammula, S. A. Feldman, M. A. Toomey, S. P. Kerkar, N. P. Restifo, J. C. Yang, S. A. Rosenberg, Tumor-infiltrating lymphocytes genetically engineered with an inducible gene encoding interleukin-12 for the immunotherapy of metastatic melanoma. *Clin. Cancer Res.* **21**, 2278–2288 (2015).
9. B. Kwong, S. A. Gai, J. Elkhader, K. D. Wittrup, D. J. Irvine, Localized immunotherapy via liposome-anchored anti-CD137 + IL-2 prevents lethal toxicity and elicits local and systemic antitumor immunity. *Cancer Res.* **73**, 1547–1558 (2013).
10. Q. Chen, C. Wang, X. Zhang, G. Chen, Q. Hu, H. Li, J. Wang, D. Wen, Y. Zhang, Y. Lu, G. Yang, C. Jiang, J. Wang, G. Dotti, Z. Gu, In situ sprayed bioresponsive immunotherapeutic gel for post-surgical cancer treatment. *Nat. Nanotechnol.* **14**, 89–97 (2019).
11. C. G. Park, C. A. Hartl, D. Schmid, E. M. Carmona, H.-J. Kim, M. S. Goldberg, Extended release of perioperative immunotherapy prevents tumor recurrence and eliminates metastases. *Sci. Transl. Med.* **10**, eaar1916 (2018).
12. J. Ishihara, A. Ishihara, K. Sasaki, S. S.-Y. Lee, J.-M. Williford, M. Yasui, H. Abe, L. Potin, P. Hosseinchi, K. Fukunaga, M. M. Raczy, L. T. Gray, A. Mansurov, K. Katsumata, M. Fukayama, S. J. Kron, M. A. Swartz, J. A. Hubbell, Targeted antibody and cytokine cancer immunotherapies through collagen affinity. *Sci. Transl. Med.* **11**, eaau3259 (2019).
13. M. Dougan, J. R. Ingram, H. J. Jeong, M. M. Mosaheb, P. T. Bruck, L. Ali, N. Pishesha, O. Blomberg, P. M. Tyler, M. M. Servos, M. Rashidian, Q.-D. Nguyen, U. H. von Andrian, H. L. Ploegh, S. K. Dougan, Targeting cytokine therapy to the pancreatic tumor microenvironment using PD-L1-specific VHHs. *Cancer Immunol. Res.* **6**, 389–401 (2018).
14. N. Momin, N. K. Mehta, N. R. Bennett, L. Ma, J. R. Palmeri, M. M. Chinn, E. A. Lutz, B. Kang, D. J. Irvine, S. Spranger, K. D. Wittrup, Anchoring of intratumorally administered cytokines to collagen safely potentiates systemic cancer immunotherapy. *Sci. Transl. Med.* **11**, eaaw2614 (2019).
15. J. M. Thomas, P. S. Daugherty, Proligands with protease-regulated binding activity identified from cell-displayed prodomain libraries. *Protein Sci.* **18**, 2053–2059 (2009).
16. O. Erster, J. M. Thomas, J. Hamzah, A. M. Jabaiah, J. A. Getz, T. D. Schoep, S. S. Hall, E. Ruoslahti, P. S. Daugherty, Site-specific targeting of antibody activity in vivo mediated by disease-associated proteases. *J. Control. Release* **161**, 804–812 (2012).
17. L. R. Desnoyers, O. Vasiljeva, J. H. Richardson, A. Yang, E. E. M. Menendez, T. W. Liang, C. Wong, P. H. Bessette, K. Kamath, S. J. Moore, J. G. Sagert, D. R. Hostetter, F. Han, J. Gee, J. Flandez, K. Markham, M. Nguyen, M. Krimm, K. R. Wong, S. Liu, P. S. Daugherty, J. W. West, H. B. Lowman, Tumor-specific activation of an EGFR-targeting probody enhances therapeutic index. *Sci. Transl. Med.* **5**, 207ra144 (2013).
18. Y. Yang, Q. Guo, X. Chen, J. Zhang, H. Guo, W. Qian, S. Hou, J. Dai, B. Li, Y. Guo, H. Wang, Preclinical studies of a pro-antibody-drug conjugate designed to selectively target EGFR-overexpressing tumors with improved therapeutic efficacy. *MAbs* **8**, 405–413 (2016).
19. I.-J. Chen, C.-H. Chuang, Y.-C. Hsieh, Y.-C. Lu, W.-W. Lin, C.-C. Huang, T.-C. Cheng, Y.-A. Cheng, K.-W. Cheng, Y.-T. Wang, F.-M. Chen, T.-L. Cheng, S.-C. Tzou, Selective antibody activation through protease-activated pro-antibodies that mask binding sites with inhibitory domains. *Sci. Rep.* **7**, 11587 (2017).
20. V. H. Trang, X. Zhang, R. C. Yumul, W. Zeng, I. J. Stone, S. W. Wo, M. M. Dominguez, J. H. Cochran, J. K. Simmons, M. C. Ryan, R. P. Lyon, P. D. Senter, M. R. Levengood, A coiled-coil masking domain for selective activation of therapeutic antibodies. *Nat. Biotechnol.* **37**, 761–765 (2019).
21. L. Sandersjöö, A. Jonsson, J. Löfblom, A new prodrug form of Affibody molecules (pro-Affibody) is selectively activated by cancer-associated proteases. *Cell. Mol. Life Sci.* **72**, 1405–1415 (2015).
22. C.-S. Pai, D. M. Simons, X. Lu, M. Evans, J. Wei, Y.-H. Wang, M. Chen, J. Huang, C. Park, A. Chang, J. Wang, S. Westmoreland, C. Beam, D. Banach, D. Bowley, F. Dong, J. Seagal, W. Ritacco, P. L. Richardson, S. Mitra, G. Lynch, P. Bousquet, J. Mankovich, G. Kingsbury, L. Fong, Tumor-conditional anti-CTLA4 uncouples antitumor efficacy from immunotherapy-related toxicity. *J. Clin. Invest.* **129**, 349–363 (2019).
23. M. Geiger, K.-G. Stubenrauch, J. Sam, W. F. Richter, G. Jordan, J. Eckmann, C. Hage, V. Nicolini, A. Freimoser-Grundschober, M. Ritter, M. E. Lauer, H. Stahlberg, P. Ringler,

J. Patel, E. Sullivan, S. Grau-Richards, S. Endres, S. Kobold, P. Umaña, P. Brünker, C. Klein, Protease-activation using anti-idiotypic masks enables tumor specificity of a folate receptor 1-T cell bispecific antibody. *Nat. Commun.* **11**, 3196 (2020).
24. K. Kitamura, T. Takahashi, T. Yamaguchi, A. Noguchi, A. Noguchi, K.-i. Takashina, H. Tsurumi, M. Inagake, T. Toyokuni, S.-i. Hakomori, Chemical engineering of the monoclonal antibody A7 by polyethylene glycol for targeting cancer chemotherapy. *Cancer Res.* **51**, 4310–4315 (1991).
25. A. Makkouk, C. Chester, H. E. Kohrt, Rationale for anti-CD137 cancer immunotherapy. *Eur. J. Cancer* **54**, 112–119 (2016).
26. D.-T. Chu, N. D. Bac, K.-H. Nguyen, N. L. B. Tien, V. V. Thanh, V. T. Nga, V. T. N. Ngoc, D. T. Anh Dao, L. N. Hoan, N. P. Hung, N. T. Trung Thu, V.-H. Pham, L. N. Vu, T. A. V. Pham, D. B. Thimiri Govinda Raj, An update on anti-CD137 antibodies in immunotherapies for cancer. *Int. J. Mol. Sci.* **20**, 1822 (2019).
27. S. J. Stocks, A. J. M. Jones, C. W. Ramey, D. E. Brooks, A fluorometric assay of the degree of modification of protein primary amines with polyethylene glycol. *Anal. Biochem.* **154**, 232–234 (1986).
28. R. A. Gatenby, R. J. Gillies, Why do cancers have high aerobic glycolysis? *Nat. Rev. Cancer* **4**, 891–899 (2004).
29. J.-Z. Du, H.-J. Li, J. Wang, Tumor-acidity-cleavable maleic acid amide (TACMAA): A powerful tool for designing smart nanoparticles to overcome delivery barriers in cancer nanomedicine. *Acc. Chem. Res.* **51**, 2848–2856 (2018).
30. P. Kuppusamy, H. Li, G. Ilangovan, A. J. Cardounel, J. L. Zweier, K. Yamada, M. C. Krishna, J. B. Mitchell, Noninvasive imaging of tumor redox status and its modification by tissue glutathione levels. *Cancer Res.* **62**, 307–312 (2002).
31. J. P. Lodolce, D. L. Boone, S. Chai, R. E. Swain, T. Dassopoulos, S. Trettin, A. Ma, IL-15 receptor maintains lymphoid homeostasis by supporting lymphocyte homing and proliferation. *Immunity* **9**, 669–676 (1998).
32. M. Ahmadzadeh, L. A. Johnson, B. Heemskerk, J. R. Wunderlich, M. E. Dudley, D. E. White, S. A. Rosenberg, Tumor antigen-specific CD8 T cells infiltrating the tumor express high levels of PD-1 and are functionally impaired. *Blood* **114**, 1537–1544 (2009).
33. J. A. Chacon, S. Pilon-Thomas, A. A. Sarnaik, L. G. Radvanyi, Continuous 4-1BB co-stimulatory signals for the optimal expansion of tumor-infiltrating lymphocytes for adoptive T-cell therapy. *Oncoimmunology* **2**, e25581 (2013).
34. M. W. Handlogten, M. Zhu, S. Ahuja, Glutathione and thioredoxin systems contribute to recombinant monoclonal antibody interchain disulfide bond reduction during bioprocessing. *Biotechnol. Bioeng.* **114**, 1469–1477 (2017).
35. D. S. Vinay, B. S. Kwon, Immunotherapy of cancer with 4-1BB. *Mol. Cancer Ther.* **11**, 1062–1070 (2012).
36. S. A. Rosenberg, N. P. Restifo, J. C. Yang, R. A. Morgan, M. E. Dudley, Adoptive cell transfer: A clinical path to effective cancer immunotherapy. *Nat. Rev. Cancer* **8**, 299–308 (2008).
37. Y. Yao, L. Li, S.-H. Yang, C.-Y. Gao, L.-H. Liao, Y.-Q. Xie, X.-Y. Yin, Y.-Q. Yang, Y.-Y. Fei, Z.-X. Lian, CD8 + T cells and IFN-γ induce autoimmune myelofibrosis in mice. *J. Autoimmun.* **89**, 101–111 (2018).
38. D. M. Willerford, J. Chen, J. A. Ferry, L. Davidson, A. Ma, F. W. Alt, Interleukin-2 receptor α chain regulates the size and content of the peripheral lymphoid compartment. *Immunity* **3**, 521–530 (1995).
39. S. Chen, L.-F. Lee, T. S. Fisher, B. Jessen, M. Elliott, W. Evering, K. Logronio, G. H. Tu, K. Tsaparikos, X. Li, H. Wang, C. Ying, M. Xiong, T. Van Arsdale, J. C. Lin, Combination of 4-1BB agonist and PD-1 antagonist promotes antitumor effector/memory CD8 T cells in a poorly immunogenic tumor model. *Cancer Immunol. Res.* **3**, 149–160 (2015).
40. P. Kubes, C. Jenne, Immune responses in the liver. *Annu. Rev. Immunol.* **36**, 247–277 (2018).
41. Y. Zen, M. M. Yeh, Hepatotoxicity of immune checkpoint inhibitors: A histology study of seven cases in comparison with autoimmune hepatitis and idiosyncratic drug-induced liver injury. *Mod. Pathol.* **31**, 965–973 (2018).
42. L. Niu, S. Strahotin, B. Hewes, B. Zhang, Y. Zhang, D. Archer, T. Spencer, D. Dillehay, B. Kwon, L. Chen, A. T. Vella, R. S. Mittler, Cytokine-mediated disruption of lymphocyte trafficking, hemopoiesis, and induction of lymphopenia, anemia, and thrombocytopenia in anti-CD137-treated mice. *J. Immunol.* **178**, 4194–4213 (2007).
43. J. S. Miller, C. Morishima, D. G. McNeel, M. R. Patel, H. E. K. Kohrt, J. A. Thompson, P. M. Sondel, H. A. Wakelee, M. L. Disis, J. C. Kaiser, M. A. Cheever, H. Streicher, S. P. Creekmore, T. A. Waldmann, K. C. Conlon, A first-in-human phase I study of subcutaneous outpatient recombinant human IL15 (rhIL15) in adults with advanced solid tumors. *Clin. Cancer Res.* **24**, 1525–1535 (2018).
44. J. Peng, Q. Yang, K. Shi, Y. Xiao, X. Wei, Z. Qian, Intratumoral fate of functional nanoparticles in response to microenvironment factor: Implications on cancer diagnosis and therapy. *Adv. Drug Deliv. Rev.* **143**, 37–67 (2019).
45. K. A. Autio, V. Boni, R. W. Humphrey, A. Naing, Probody therapeutics: An emerging class of therapies designed to enhance on-target effects with reduced off-tumor toxicity for use in immuno-oncology. *Clin. Cancer Res.* **26**, 984–989 (2020).
46. D. Giesen, L. N. Broer, M. N. Lub-de Hooge, I. Popova, B. Howng, M. Nguyen, O. Vasiljeva, E. G. E. de Vries, M. Pool, Probody therapeutic design of $^{89}$Zr-CX-072 promotes accumulation in PD-L1-expressing tumors compared to normal murine lymphoid tissue. *Clin. Cancer Res.* **26**, 3999–4009 (2020).
47. Q. Yao, L. Kou, Y. Tu, L. Zhu, MMP-responsive 'smart' drug delivery and tumor targeting. *Trends Pharmacol. Sci.* **39**, 766–781 (2018).
48. J. L. Major Jourden, S. M. Cohen, Hydrogen peroxide activated matrix metalloproteinase inhibitors: A prodrug approach. *Angew. Chem. Int. Ed.* **49**, 6795–6797 (2010).
49. T. Legigan, J. Clarhaut, I. Tranoy-Opalinski, A. Monvoisin, B. Renoux, M. Thomas, A. Le Pape, S. Lerondel, S. Papot, The first generation of β-galactosidase-responsive prodrugs designed for the selective treatment of solid tumors in prodrug monotherapy. *Angew. Chem. Int. Ed.* **51**, 11606–11610 (2012).
50. N.-C. Fan, F.-Y. Cheng, J.-A. Ho, C.-S. Yeh, Photocontrolled targeted drug delivery: Photocaged biologically active folic acid as a light-responsive tumor-targeting molecule. *Angew. Chem. Int. Ed.* **51**, 8806–8810 (2012).
51. F. Zhou, T. Fu, Q. Huang, H. Kuai, L. Mo, H. Liu, Q. Wang, Y. Peng, D. Han, Z. Zhao, X. Fang, W. Tan, Hypoxia-activated PEGylated conditional aptamer/antibody for cancer imaging with improved specificity. *J. Am. Chem. Soc.* **141**, 18421–18427 (2019).
52. W. Engelen, K. Zhu, N. Subedi, A. Idili, F. Ricci, J. Tel, M. Merkx, Programmable bivalent peptide-DNA locks for pH-based control of antibody activity. *ACS Cent. Sci.* **6**, 22–31 (2020).
53. L. Tang, Y. Zheng, M. B. Melo, L. Mabardi, A. P. Castaño, Y.-Q. Xie, N. Li, S. B. Kudchodkar, H. C. Wong, E. K. Jeng, M. V. Maus, D. J. Irvine, Enhancing T cell therapy through TCR-signaling-responsive nanoparticle drug delivery. *Nat. Biotechnol.* **36**, 707–716 (2018).
54. A. M. Deshpande, A. A. Natu, N. P. Argade, Chemoselective carbon–carbon coupling of organocuprates with (bromomethyl)methylmaleic anhydride: Synthesis of chaetomellic acid A. *J. Org. Chem.* **63**, 9557–9558 (1998).
55. K. Maier, E. Wagner, Acid-labile traceless click linker for protein transduction. *J. Am. Chem. Soc.* **134**, 10169–10173 (2012).
56. S. N. Wood, Fast stable restricted maximum likelihood and marginal likelihood estimation of semiparametric generalized linear models. *J. R. Stat. Soc. Ser. B* **73**, 3–36 (2011).

**Acknowledgments:** We thank D. J. Irvine (MIT, MA, USA) for providing the IL-15SA plasmid. We acknowledge the EPFL Molecular and Hybrid Materials Characterization Centre, Nuclear Magnetic Resonance spectroscopy facilities, Centre of PhenoGenomics, Flow Cytometry Core Facility, and Protein Production and Structure Core Facility for technical assistance. The graphic illustrations in Figs. 1 and 2 and supplementary figures were created with BioRender.com. **Funding:** This work was supported, in part, by the Swiss National Science Foundation (SNSF Project grant 315230_173243), ISREC Foundation with a donation from the Biltema Foundation, Swiss Cancer League (no. KFS-4600-08-2018), the European Research Council under the ERC grant agreement MechanoIMM (805337), Kristian Gerhard Jebsen Foundation, Foundation Pierre Mercier pour la science, Anna Fuller Fund Grant, and EPFL. Y.Z. is supported by the Eurotech Postdoctoral Programme that is cofounded by the European Commission under its framework program Horizon 2020 (grant agreement 754462). M.G. is supported by the Chinese Scholarship Council (CSC, No. 201808320453). S.V.H. is supported by a Ghent University—Special Research Found (BOF PDO.2009.0006.01) postdoctoral fellowship and FWO travel grant (V412920N). **Author contributions:** Y.Z. and L.T. conceived the study. Y.Z., Y.-Q.X., and L.T. designed the experiments. Y.Z. and S.V.H. prepared and characterized the materials. Y.Z., Y.-Q.X., and S.V.H. performed the in vitro and in vivo experiments. M.G. and Y.G. prepared IL-15SA. S.N. performed the data analysis with scatterplot smoothing. Y.Z., Y.-Q.X., and L.T. analyzed the data and wrote the manuscript. All authors edited the manuscript. **Competing interests:** The authors declare that they have no competing interests. **Data and materials availability:** All data needed to evaluate the conclusions in the paper are present in the paper and/or the Supplementary Materials.

Submitted 24 January 2021
Accepted 21 July 2021
Published 10 September 2021
10.1126/sciadv.abg7291

**Citation:** Y. Zhao, Y.-Q. Xie, S. Van Herck, S. Nassiri, M. Gao, Y. Guo, L. Tang, Switchable immune modulator for tumor-specific activation of anticancer immunity. *Sci. Adv.* **7**, eabg7291 (2021).

ScienceAdvances

# Switchable immune modulator for tumor-specific activation of anticancer immunity

Yu ZhaoYu-Qing XieSimon Van HerckSina NassiriMin GaoYugang GuoLi Tang

*Sci. Adv.*, 7 (37), eabg7291. • DOI: 10.1126/sciadv.abg7291



*Science Advances* (ISSN ) is published by the American Association for the Advancement of Science. 1200 New York Avenue NW, Washington, DC 20005. The title *Science Advances* is a registered trademark of AAAS.